

# Optimal Micro-Vane Flow Control for Compact Air Vehicle Inlets

Bernhard H. Anderson  
Glenn Research Center, Cleveland, Ohio

Daniel N. Miller  
Lockheed Martin Aerospace Company, Fort Worth, Texas

Gregory A. Addington  
Wright-Patterson Air Force Base, Dayton, Ohio

Johan Agrell  
Swedish Defence Research Agency, Bromma, Sweden

## The NASA STI Program Office . . . in Profile

Since its founding, NASA has been dedicated to the advancement of aeronautics and space science. The NASA Scientific and Technical Information (STI) Program Office plays a key part in helping NASA maintain this important role.

The NASA STI Program Office is operated by Langley Research Center, the Lead Center for NASA's scientific and technical information. The NASA STI Program Office provides access to the NASA STI Database, the largest collection of aeronautical and space science STI in the world. The Program Office is also NASA's institutional mechanism for disseminating the results of its research and development activities. These results are published by NASA in the NASA STI Report Series, which includes the following report types:

- **TECHNICAL PUBLICATION.** Reports of completed research or a major significant phase of research that present the results of NASA programs and include extensive data or theoretical analysis. Includes compilations of significant scientific and technical data and information deemed to be of continuing reference value. NASA's counterpart of peer-reviewed formal professional papers but has less stringent limitations on manuscript length and extent of graphic presentations.
- **TECHNICAL MEMORANDUM.** Scientific and technical findings that are preliminary or of specialized interest, e.g., quick release reports, working papers, and bibliographies that contain minimal annotation. Does not contain extensive analysis.
- **CONTRACTOR REPORT.** Scientific and technical findings by NASA-sponsored contractors and grantees.

- **CONFERENCE PUBLICATION.** Collected papers from scientific and technical conferences, symposia, seminars, or other meetings sponsored or cosponsored by NASA.
- **SPECIAL PUBLICATION.** Scientific, technical, or historical information from NASA programs, projects, and missions, often concerned with subjects having substantial public interest.
- **TECHNICAL TRANSLATION.** English-language translations of foreign scientific and technical material pertinent to NASA's mission.

Specialized services that complement the STI Program Office's diverse offerings include creating custom thesauri, building customized databases, organizing and publishing research results . . . even providing videos.

For more information about the NASA STI Program Office, see the following:

- Access the NASA STI Program Home Page at <http://www.sti.nasa.gov>
- E-mail your question via the Internet to [help@sti.nasa.gov](mailto:help@sti.nasa.gov)
- Fax your question to the NASA Access Help Desk at 301-621-0134
- Telephone the NASA Access Help Desk at 301-621-0390
- Write to:  
NASA Access Help Desk  
NASA Center for Aerospace Information  
7121 Standard Drive  
Hanover, MD 21076



# Optimal Micro-Vane Flow Control for Compact Air Vehicle Inlets

Bernhard H. Anderson  
Glenn Research Center, Cleveland, Ohio

Daniel N. Miller  
Lockheed Martin Aerospace Company, Fort Worth, Texas

Gregory A. Addington  
Wright-Patterson Air Force Base, Dayton, Ohio

Johan Agrell  
Swedish Defence Research Agency, Bromma, Sweden

National Aeronautics and  
Space Administration

Glenn Research Center

This work was sponsored by the Low Emissions Alternative  
Power Project of the Vehicle Systems Program at the  
NASA Glenn Research Center.

Available from

NASA Center for Aerospace Information  
7121 Standard Drive  
Hanover, MD 21076

National Technical Information Service  
5285 Port Royal Road  
Springfield, VA 22100

Available electronically at <http://gltrs.grc.nasa.gov>

# OPTIMAL MICRO-VANE FLOW CONTROL FOR COMPACT AIR VEHICLE INLETS

Bernhard H. Anderson  
National Aeronautics and Space Administration  
Glenn Research Center  
Cleveland, Ohio 44135

Daniel N. Miller  
Lockheed Martin Aerospace Company  
Fort Worth, Texas 76101

Gregory A. Addington  
Wright-Patterson Air Force Base  
Dayton, Ohio 45433

Johan Agrell  
Swedish Defence Research Agency  
Bromma, Sweden SE-17290

## ABSTRACT

The purpose of this study on micro-vane secondary flow control is to demonstrate the viability and economy of *Response Surface Methodology* (RSM) to optimally design micro-vane secondary flow control arrays, and to establish that the aeromechanical effects of engine face distortion can also be included in the design and optimization process. These statistical design concepts were used to investigate the design characteristics of “low unit strength” micro-effector arrays. “Low unit strength” micro-effectors are micro-vanes set at very low angles-of-incidence with very long chord lengths. They were designed to influence the near wall inlet flow over an extended streamwise distance, and their advantage lies in low total pressure loss and high effectiveness in managing engine face distortion. Therefore, this report examines optimal micro-vane secondary flow control array designs for compact inlets through a *Response Surface Methodology*.

## INTRODUCTION

The current development strategy for combat air-vehicles is directed towards reduction in the Life-Cycle Cost (LCC) with little or no compromise to air-vehicle performance and survivability. This strategy has been extended to the aircraft component level, in particular, the engine inlet diffuser system. One method to reduce inlet system LCC is to reduce its structural weight and volume. Consequently, advanced combat inlet configurations are being made more compact (or shorter) to achieve weight and volume (and LCC) reduction. However, compact S-duct diffusers are characterized by high distortion and low pressure recovery produced by extreme wall curvature and strong secondary flow gradients. These characteristics are further aggravated by maneuver conditions. The requirement to highly integrate or embed the propulsion system often leads to conformal inlet aperture shapes which do not lend themselves to good aerodynamic performance. These configurations also present a challenging environment for both fan/compressor surge margin and aeromechanical vibration. Interest in High Cycle Fatigue (HCF) research by the US aerospace community has been spurred by discrepancies between the expected durability of engine components compared to that actually experienced in the field. Recognizing that inlet distortion is a forcing function for vibration in the fan components, methods for increasing HCF

Life Expectancy can be combined with techniques for inlet recovery and engine face distortion management. Therefore, to enable acceptable performance levels in such advanced, compact inlet diffuser configurations, microscale secondary flow control methods are being developed to manage the recovery, distortion, and HCF aspects of these complex flow fields.<sup>(1)-(2)</sup>

One of the most difficult tasks in the design of microscale arrays for optimal inlet operation is arriving at the geometric placement, arrangement, number, size and orientation of the effector devices within the inlet duct to achieve optimal performance. These effector devices can be activated by either mechanical or fluidic means. This task is complicated not only by the large number of possible design variables available to the aerodynamicist, but also by the number of decision parameters that are brought into the design process. By including the HCF effects in the inlet design process, the aerodynamicist has a total of seven individual response variables which measure various aspect of inlet performance. They include the inlet total pressure recovery, the inlet total pressure recovery distortion at the engine face and the first five Fourier harmonic 1/2 amplitudes of distortion. Each of these responses need to be either maximized, minimized, constrained or unconstrained while searching for the optimal combination of primary design variable values that satisfy the mission requirements. The design task is further complicated by the existence of hard-to-control factors which effect inlet performance, i.e. the mission variables. The design of inlet systems is usually accomplished at the cruise condition (the on-design condition) while variations from the cruise condition are considered as an off-design penalty. The mission variables that cause the off-design penalty are, for example, inlet throat Mach number (engine corrected weight flow), angle-of-incidence and angle-of-yaw. Numerical optimization procedures that have been successful with some aerodynamic problems give little assistance to the design of microscale secondary flow arrays. It is very difficult to incorporate large numbers of independent design and response variables into such procedures. Further, they are very expensive to use if the individual Computational Fluid Dynamics (CFD) experiments are solutions to the full Navier-Stokes equations in three dimensions. However, there is a statistical approach to the problem which combines an optimally sequenced pattern of Design-of-Experiments (DOE), statistical model building, and system optimization called *Response Surface Methodology* (RSM). It is ideally suited to the design of micro-vane arrays for optimal inlet performance, particularly when multiple design objectives are present.

In the 1950s and 1960s, Box<sup>(3)-(4)</sup> and co-workers developed a collection of analytical and statistical experimental design tools for which the term *Response Surface Methodology* (RSM) was coined. RSM provides an economical, reliable and systematic approach to variable screening as well as the general exploration of the region that contains the estimated optimal conditions. As a result, the pragmatic use of RSM places a high priority on obtaining a better understanding of the process system as well as estimating the optimum conditions. In the design of microscale secondary flow arrays for inlets, it is just as important to understand and quantify the behavior of the design parameters in the neighborhood of the optimal conditions as to know the optimal conditions. Hence, an RSM approach is particularly beneficial for the design of micro-vane arrays since there are a great many design variables available to the aerodynamicist, and often there exists multiple design objectives. Another critical aspect of RSM is its ability to study statistical interactions among the design variables. These interactions often indicate a potential for achieving a robust control factor combination. A robust control factor combination is one for which variations in the individual factors has minimal effect on the response variables. The robustness increases as the tolerable variation in the design factors increases.

A statistical interaction exists between two independent factor variables  $X_1$  and  $X_2$  when the effect of  $X_1$  on response  $Y_i$  is affected by the value of  $X_2$ . In other words, the effect of factor  $X_1$  on response  $Y_i$  is not unique, but changes as a function of factor  $X_2$ . This is often called a synergistic effect, and it is very important in micro-vane array design. In addition, it is often desirable in inlet design to satisfy several objectives at one time. For example, in designing an inlet for HCF considerations, it may be desirable to determine the combination of factor settings that maximize inlet total pressure recovery, minimize engine face distortion, and constrain a particular Fourier harmonic 1/2 amplitude of distortion to a given safe value at the natural resonance frequency of the engine fan blades. However, since the resonance frequency of the engine blades is not generally known, the desired design goal may be to collectively reduce all the Fourier harmonic 1/2 amplitudes of engine face distortion.

In this research study on micro-vane flow control, three objectives were considered important, namely: (1) to determine the design characteristics of micro-vane secondary flow control arrays, (2) to establish the ability of micro-vanes to manage the aeromechanical effects of engine face distortion, and (3) to evaluate the effectiveness of robust parameter design methodologies for high performance “open loop” micro-vane arrays designs over a range of throat Mach numbers and angle-of-incidences. This report covers the first two research objectives while Anderson, Baust, and Agrell<sup>(5)</sup> covers the third objective and describes a design methodology whereby the hard-to-control mission variables are explicitly included in the design of optimal robust micro-vane arrays.

## NOMENCLATURE

AIP	Aerodynamic Interface Plane
$c$	Effector Chord Length
CCF	Central Composite Face-Centered
CFD	Computational Fluid Dynamics
$D$	Engine Face Diameter
DC60	Circumferential Distortion Descriptor
DOE	Design of Experiments
$h$	Effector Blade Height
HCF	High Cycle Fatigue
$F_{k/2}$	$k^{\text{th}}$ Fourier Harmonic 1/2-Amplitude
$FM/2$	Mean Fourier Harmonic 1/2-Amplitude
$L$	Inlet Diffuser Length
LCC	Life Cycle Costs
MSFC	microscale Secondary Flow Control
$M_t$	Inlet Throat Mach Number
$n$	Number of Effector Vanes per Band
PFAVE	Average Inlet Total Pressure at AIP
PAVCRT	Minimum Total Pressure over Critical Sector Angle at AIP
QAVE	Average Dynamic Pressure at AIP
$R$	Inlet Radius
$R_{cl}$	Centerline Radius
$R_{ef}$	Engine Face Radius
$R_{thr}$	Inlet Throat Radius

ROC	Robust Optimization Concepts
Re	Reynold Number per ft.
RSM	Response Surface Methodology
S	Standard Deviation
S <sub>clock</sub>	Standard Deviation over the Rake Clocking Angles
UAV	Unmanned Air Vehicle
UCAV	Unmanned Combact Air Vehicle
X <sub>cl</sub>	Axial Distance Along the Duct Centerline
Y <sub>A</sub>	Upper 95% Confidence Interval Predicted by DOE Analysis
Y <sub>CFD</sub>	Response Predicted by CFD Analysis
Y <sub>DOE</sub>	Response Predicted by DOE Analysis
Y <sub>i,j</sub>	Generalized Response Variable
Z <sub>cl</sub>	Centerline Offset Displacement
α	Inlet Angle-of-Incidence
ΔZ <sub>cl</sub>	Inlet Centerline Offset

## RESULTS AND DISCUSSION

### Baseline Flow in the Redesigned M2129 Inlet S-Duct

The redesigned M2129 inlet S-duct used in this study was considered similar to the original DERA/M2129 inlet S-duct defined by AGARD FDP Working Group 13 Test Case 3,<sup>(6)</sup> using Lip No. 3 and Forward Extension No. 2. This inlet design was first proposed by Willmer, Brown and Goldsmith,<sup>(7)</sup> and has been used extensively in the US and UK to explore inlet flow control array design. The centerline for the redesigned M2129 inlet is given by the equation

$$Z_{cl} = -\frac{\Delta Z_{cl}}{2} \left( 1 - \cos \left( \pi \cdot \frac{X_{cl}}{L} \right) \right) \quad (1)$$

The radius distribution measured normal to the inlet centerline is given by the expression

$$\left( \frac{R_{cl} - R_{thr}}{R_{ef} - R_{thr}} \right) = 3 \left( 1 - \frac{X_{cl}}{L} \right)^4 - 4 \left( 1 - \frac{X_{cl}}{L} \right)^3 + 1 \quad (2)$$

where  $R_{thr} = 2.5355$  inches,  $R_{ef} = 3.0$  inches,  $L = 15.0$  inches, and  $\Delta Z_{cl} = 5.7809$  inches. The redesign of the M2129 inlet was such that the new inlet matches the static pressure gradients normally found in typical UAV or UCAV designs. Therefore, the new inlet is more compact than the original M2129 inlet S-duct. As a consequence, supersonic flow will develop in this inlet when the inlet throat Mach number increases much above 0.70. The geometry and grid structure for the resigned M2129 inlet S-duct is described in detail in Anderson, Baust, and Agrell.<sup>(5)</sup>

Traditionally, this type of compact inlet duct would be excluded from design consideration since it is characterized by severe wall curvature that induces strong secondary flows. These strong secondary flow can cause a flow separation called vortex lift-off. See Figure (1).

This type of 3D flow separation results in severe total pressure losses and engine face distortion. Figure (2) presents the engine face total pressure recovery contours and secondary flow velocity vectors for the redesigned DERA/M2129 inlet S-duct at a throat Mach number of 0.70. A vortex pair is dominant in the engine face flow field, and this was accompanied by very severe engine face total pressure distortion.

### **Inlet Flow Control Micro-Vane Effector Design Approach**

In the “secondary flow control” concept, microscale actuation is used as an approach to alter the inlet S-duct’s inherent secondary flow with the goal of simultaneously improving the critical system level performance metrics of total pressure recovery, engine face distortion, and HCF characteristics. In studying the influence of micro-vane chord length<sup>(1)</sup> on inlet performance, it was determined that this factor was very important parameter in reducing engine face distortion as well as managing the harmonic content of engine face distortion. While there appear to be limits on the total number and strength of the individual effector units<sup>(1)</sup> in managing engine face distortion, there appear to be no such limits on micro-vane chord length. By installing multiple bands of micro-effector units, the chord length can be effectively increased,<sup>(8-10)</sup> and engine face distortion managed. However, this improvement in engine face distortion came at the expense of total pressure recovery. In order to overcome the dimensional limit of chord length, the micro-vane angle of incidence can be greatly reduced while compensating by increasing the length of the micro-vane effector units. Hence effective inlet flow control management of engine face distortion can be achieved by reducing the unit strength of the vane effector and allowing the array design to influence the inlet flow over an extended streamwise distance. With this combination, the total pressure losses associated with micro-vane effectors become very small, and a large overall performance gain can be achieved.<sup>(5)</sup>

### **Inlet Flow Control Micro-Vane Effector Array Design**

To manage the flow in the redesigned M2129 inlet S-duct, a single band array arrangement of microscale effectors was placed in the upstream section near the inlet throat. See Figures (3) and (4). These microscale effectors were micro-vanes, the largest height being about the average height of the momentum layer just downstream of the inlet throat or about 2.0 mm. The purpose of these micro-vanes was to create a set of co-rotating vortices that would quickly merge to form a thin layer of secondary flow that will counter the formation of the passage vortex pair. Since the height of the vane effectors were limited to 2.0 mm, a single-band arrangement of micro-vanes set at 5.0° angle-of-incidence was chosen to investigate the enhancing effect of increasing the vane chord length on distortion management, i.e. allowing the array design to influence the inlet flow over an extended streamwise distance for a design advantage

The DOE approach followed directly from the objectives previously stated and was reflected in the layout of the design factors listed in Table (1). The factor variables were the number of vane effector units ( $n$ ), the micro-vane effector height ( $h$ ), and the micro-vane chord length Table (2) shows the variables that were held constant during this study. They include the effector vane thickness ( $t$ ), the geometric angle-of-incidence of the micro vanes ( $\beta$ ), the inlet operating total pressure ( $P_t$ ) and total temperature ( $T_t$ ), the inlet throat Mach Number ( $M_t$ ), the inlet angle-of-incidence ( $\alpha$ ), and the inlet angle-of-yaw ( $\gamma$ ). Table (3) displays the response variables

for this study. They include the inlet total pressure recovery (PFAVE), the engine face distortion (DC60), and the first five Fourier harmonic 1/2-amplitudes of engine face distortion (F1/2, F2/2, F3/2, F4/2, and F5/2).

The DOE strategy selected was a Central Composite Face-Centered (CCF) DOE. This strategy resulted in 15 unique CFD experimental cases that are shown in Table (4). This particular DOE, like most DOE strategies, varied more than one factor at a time. Further, this layout of 15 cases permitted the estimation of both linear and curvilinear effects as well as two-factor interactive or synergistic effects among the DOE factors. This CCF DOE strategy is superior to the traditional approach of changing one variable at a time because that approach does not permit the estimation of the two-factor interactions.

A graphical representation of the Central Composite Face-Centered DOE used in the study is presented in Figure (5). The DOE cases are represented in this figure by the circular symbols, where the symbol locations on the cube signify the factor values. This DOE is called a composite DOE because the cases are composed of a fractional factorial part and a quadratic part. The full-fractional factorial part of the DOE is composed of the  $2^3$  or 8 cases which are represented by the eight corner locations on the cube in Figure (5). The remaining cases in Figure (5) are the quadratic part of the DOE. These cases allow for the evaluation of the curvilinear effects. All together, there are a total of 15 cases in a Central Composite Face-Centered DOE with three factor variables. Notice the balanced layout of cases in Figure (5). This layout of cases represents the smallest number of CCF DOE cases that allows for the evaluation of linear and curvilinear effects as well as all two-factor interactive or synergistic effects.

Each of the 15 cases in Table (4) was run with a Reynolds-averaged Navier-Stokes code<sup>(11)</sup> that allowed for numerical simulation of micro-vane effectors without the need to physically embed the vane effectors within the CFD grid structure. However, for the present study the individual vanes were incorporated into the half cylindrical grid structure. The micro-vanes all had a thickness of 0.138 mm. See Table (2). The computational grid surrounding the micro-vanes was developed such that it reasonably resolved the boundary layer development on both the suction and pressure surfaces of each micro-vane in the array. Because wall functions were used in the calculations, the grid resolution for the individual micro-vanes was simplified. However, the boundary layer along the micro-vane edges was assumed to be negligible, and therefore not resolved in the computational grid. The half cylindrical grid structure was composed of three blocks: an upstream block, an effector section containing the micro-vanes, and a downstream block. See Figures (3) and (4). The computational half-plane grid varied in total number of mesh points from about 950,000 to 1,150,000 depending on the micro-vane configuration. All CFD calculations were accomplished assuming half cylindrical symmetry. A two-equation k- $\epsilon$  turbulence model was used in this study. The model consists of a transport equation for the turbulent kinetic energy and turbulent length scale. This model also includes a near-wall model and compressible corrections for high speed flows.

### **Harmonic Analysis of Distortion**

The overall methodology used to obtain the harmonic content of inlet distortion was first proposed by Ludwig<sup>(12)</sup>. This methodology is characterized by the use of radial weighting factors applied to the total pressure rake measurements. The radial weighting factors are shown in Table (7). These radial weighting factors compress the rake information to a single radius

ring of data samples, where the number of data samples corresponds to the number of arms of the measurement rake. A separate study was initiated by Anderson and Keller<sup>(13)</sup> to evaluate the impact of rake geometry (specifically the number of rake arms) on the measurement error associated with estimating the first five Fourier harmonic 1/2-amplitudes of engine face distortion. As a result of that study, the rake and methodology chosen for this study was the 80-probe “clocked” AIP rake because it provided the lowest error in estimating the first five Fourier harmonic 1/2-amplitudes of engine face distortion. Clocking the AIP rake means that N separate measurements were taken, and at each separate measurement, the angular orientation of the rake was advanced by an amount 1/N times the rake angle. The rake angle is the ratio of 360° divided by the number of arms in the AIP rake. For example, a standard 80-probe rake has 16-arms. Hence the rake angle is 22.5°. Therefore total pressure measurements were obtained at each 22.5°/N angular position of the rake. Using the AIP instrumentation locations for the 80-probe rake, the 15 CFD solutions were interpolated at each of the probe positions shown in Figure (6a). The span-weighted average total pressure was calculated for the 80-probe rake by multiplying the probe total pressure by the span-weighted coefficients from Table (5), and adding the results over the five probes of the rakes to form a single radius ring of data samples.

Since the rake at the engine face was “clocked”, a complete set of “repeats” was generated at each experimental run in Table (4). From the engine face patterns at each of the 10 clocking angles, a Fourier analysis was performed on the sample set of data and a standard deviation of the “repeats”,  $S_{\text{clock}}$ , was determined for each of the Fourier harmonic 1/2-amplitudes. In order to check the constant variance assumption associated with least square regression, a simple F-test for comparing the minimum standard deviation to the maximum standard deviation ( $F = S_{\text{max}}^2/S_{\text{min}}^2$ ) was conducted for each of the five responses. The results are presented in Table (6). Since each F-test exceeded the 95% confidence critical value of  $F(0.975,9,9) = 4.03$ , the assumption of constant variance across the design space had to be discarded. This meant that a regression technique known as weighted least squares regression had to be employed for analyzing the  $10 \times 15 = 150$  data samples in the DOE. The weights in these regression analyses were set to  $1/S_{\text{clock}}^2$ .

The data reduction for the inlet total pressure recovery and engine face distortion differed greatly from the harmonic analysis of distortion described. There exists no recognized methodology to evaluate the Fourier harmonic 1/2-amplitudes of engine face distortion for more than five probes in the radial direction. Hence, evaluating the Fourier harmonic 1/2-amplitude directly from the computational mesh had to be discarded. However, both the inlet total pressure recovery and engine face distortion can and were calculated directly from the computational grid at the engine face station. This computational mesh was composed of 49 x 121 grid points in the full-plane. The DC60 engine face distortion descriptor is defined such that it can be determined from either a computational grid or a standard measurement rake.<sup>(14)</sup> It is the only recognized distortion descriptor that has this property, and hence, was chosen for this study. The DC60 engine face distortion descriptor is a measure of the difference between the engine face or AIP average total pressure (PFAVE) and the lowest average total pressure in any sector defined by a critical angle of 60° (PAVCRIT), divided by the average dynamic pressure at the engine (AIP) face. Hence,

$$\text{DC60} = \frac{(\text{PFAVE} - \text{PAVCRIT})}{\text{QAVE}} \quad (3)$$

The CFD performance results for the Central Composite Face-Centered DOE format involving the factor (design) variables are presented in Table (7). The inlet recovery (PFAVE) and the engine face distortion (DC60) were determined from the computation mesh. The Fourier harmonics 1/2-amplitudes of engine face distortion listed in Table (7) were determined from a “clocked” engine face rake and are the mean values over the 10 clocking angles. However, these values were not used in the regression analysis since weighted regression were required as a result of a lack of constant variance across the design space. Instead, the complete set of  $10 \times 15 = 150$  values together with their corresponding weighting factors were used in the weighted regression to obtain the response surfaces for each of the Fourier harmonic 1/2-amplitudes of distortion. The engine face total pressure recovery contours for the Central Composite Face-Centered DOE shown in Table (7) is presented in Figure (7).

### Interactions Between the Factor Variables

The significant terms in the DOE regression model for inlet total pressure recovery (PFAVE) are shown in Table (8), while the significant terms in the DOE regression model for the engine face distortion (DC60) are shown in Table (9). There were two important two-factor interactions identified for inlet total pressure recovery regression model and three important two-factor interactions identified for the DC60 distortion regression model. See Tables (8) and (9). For inlet total pressure recovery, the (n\*h) and (h\*c) were considered as being significant, while the (n\*h), (n\*c) and (h\*c) two-factor interaction were revealed to be important for the engine face distortion regression model. Each p-value listed on Tables (8) and (9) is defined as the probability of observing an absolute t-value that is greater than one calculated when there is no effect present. The regression models listed in Tables (8) and (9) were obtained from a backward elimination. Backwards elimination begins with the full model and deletes or eliminates the least significant term in the model until all terms left in the model are statistically significant. In the models listed in Tables (8) and (9), all terms with a significant level  $p \leq 0.10$  were retained. The relationship between p and % Signif is given by the expression:

$$\% \text{ Signif} = 100.0(1.0 - p) \quad (4)$$

Therefore, the DOE regression model only includes terms that are statistically significant.

A statistical interaction exists between two independent factor variables X1 and X2 when the effect of X1 on response Yi is affected by the value of X2. In other words, the effect of factor X1 on response Yi is not unique, but changes as a function of factor X2. For example, Figures (8) and (9) presents the inlet performance metrics PFAVE and DC60 as a function of the micro-vane effector height (h) at three levels of the number of micro-vane effectors (n). However, the rate of increase of PFAVE and the rate of decrease of DC60 as a function of micro-vane effector height (h) depended on the number of micro-vane effectors (n). See Figures (8) and (9). In fact, the (n\*h) interaction for both PFAVE and DC60 are considered strong interactions. At a micro-vane effector height (n) of 1.0 mm, the recovery increases with increasing number of micro-vane effectors (n), while the DC60 engine face distortion decreases with increasing number of micro-vane effectors (n). However, at a micro-vane effector height (n) of 2.0 mm, these trends are reverse for both inlet pressure recovery (PFAVE) and engine face distortion (DC60).

Presented in Figures (10) and (11) are the effects of micro-vane chord length (c) on inlet total pressure recovery and engine face distortion respectively for three levels of the number of micro-vane effectors (n). Since the functional relationship between PFAVE and (c) differed only by an additive constant between the three levels of (n), there was no significant (n\*c) statistical interaction for the inlet total pressure recovery (PFAVE). This is substantiated in Table (8). However, there was a (n\*c) statistical two-way interaction for the DC60 engine face distortion response variable. See Figure (11). The rate of decrease of DC60 engine face distortion as a function of micro-vane chord length (c) changes as the number of micro-vane effectors (n) were increased.

The two-factor (h\*c) statistical interaction that were indicated in Tables (8) and (9) was also observed in Figures (12) and (13) for both inlet total pressure recovery and DC60 engine face distortion. The amount of variations caused by the (h\*c) two-way interaction for engine face distortion were about the same as the (n\*h) interaction presented in Figures (9).

### Optimal Flow Control for Three Missions

To illustrate the potential of RSM to select an optimal micro-vane array design, three mission strategies were considered for the subject inlet, namely (1) Maximum Performance, (2) Maximum Engine Stability, and (3) Maximum HCF Life Expectancy. The Maximum Performance mission minimized the inlet total pressure losses, the Maximum Engine Stability mission minimized the engine face distortion, while the Maximum HCF Life Expectancy mission minimized the mean of the first five Fourier harmonic amplitudes, i.e. “collectively” reduced all the harmonic 1/2-amplitudes of engine face distortion. Each of the mission strategies was subject to a low engine face distortion constraint, i.e.  $DC60 < 0.10$ , which is a level acceptable for commercial engines, and a constraint on each individual Fourier harmonic 1/2-amplitudes:  $Fk/2 < 0.015$ ,  $k = 1, 2, \dots, 5$ .

**Maximum Performance Mission** - To obtain the Optimal Maximum Performance array design, a search was made of the factor design space to locate the factor combination that minimized the inlet duct losses:

$$Y = (1.0 - PFAVE) \quad (5)$$

subject to the constant that

$$DC60 \leq 0.10 \quad (6)$$

and that the individual Fourier harmonic 1/2-amplitudes of engine face distortion were each constrained to

$$\frac{Fk}{2} \leq 0.015 \quad (7)$$

**Maximum Engine Stability Mission** - In a like manner, the Optimal Maximum Engine Stability array design was obtained through a search process over the factor design space to locate the factor combination that minimized decision parameter:

$$Y = (DC60) \quad (8)$$

subject to the condition that the individual Fourier harmonic 1/2-amplitudes of engine face distortion were each constrained to

$$\frac{F_k}{2} \leq 0.015 \quad (9)$$

while the total pressure recovery (PFAVE) was unconstrained.

**Maximum HCF Life Expectancy Mission** -The Optimal Maximum HCF Life Expectancy MSFC array was determined through a search process over the factor variable space to locate that array geometry that minimized the mean of the first five Fourier harmonic 1/2-amplitudes of distortion, i.e

$$Y = \frac{1}{5} \sum_{k=1}^5 \left( \frac{F_k}{2} \right) \quad (10)$$

subject to the constant that

$$DC60 \leq 0.10 \quad (11)$$

and that the individual Fourier harmonic 1/2-amplitudes of engine face distortion were each constrained to

$$\frac{F_k}{2} \leq 0.015 \quad (12)$$

while the total pressure recovery (PFAVE) was unconstrained in the search procedure.

### Comparison of the Optimal Array Designs

Presented in Table (10) are the results of the search process over the factor design space for the three missions, i.e. the Maximum Performance, the Maximum Engine Stability, and the Maximum HCF Life expectancy, to arrive at the optimal array designs as predicted by the DOE regression model., A series of three CFD validation cases listed in Table (1) were run using the optimal factor combinations determined by the DOE regression models. The CFD engine face performance results are presented in Table (11). Therefore, Tables (10) and (11) present the optimal engine face performance results for each of the three missions as determined from the DOE predictions and by the CFD analyses. Seven response variables are listed in Tables (10) and (11). They include the inlet total pressure (PFAVE), the engine face distortion (DC60), the first five Fourier harmonic 1/2 amplitudes of distortion (F1/2, F2/2, F3/2, F4/2, F5/2). The mean of the first five Fourier harmonic 1/2 amplitudes of distortion (FM/2) was determined from the expression:

$$\frac{FM}{2} = \frac{1}{5} \sum_{k=1}^5 \left( \frac{Fk}{2} \right) \quad (13)$$

Comparisons of the performance of the three “Optimal Robust” array designs, i.e. the Maximum Performance, Maximum Engine Stability, and Maximum HCF Life Expectancy mission designs listed in Tables (10) and (11) indicates that performance of the three optimal array designs are remarkably similar. It is also true that the performance predicted by the DOE regression is also remarkably similar to the CFD analysis for each of the missions. This visual similarity will be studied objectively in the section entitled “Statistical Comparison of the CFD Analysis and DOE Predictions”.

Figure (14) presents a comparison of the engine face total pressure recovery contours and secondary flow field for each of the validation solutions obtained from the CFD solutions. Although the three “Optimal Robust” array designs were generated from three very different mission strategies, the engine face flow field achieved by these array designs were not visually significantly different. Presented in Figures (15) through (17) are the near wall streamlines for the three optimal array designs, i.e. the Maximum Performance, the Maximum Engine Stability, and the Maximum HCF Life expectancy missions. Shown in these figures are both the near wall streamlines for the entire inlet as well as an enlarge image of the effector region near wall streamlines.

### **Comparison of Optimal Micro-Vane and Optimal Micro-Jet Designs**

Comparison of the performance of the three “Optimal Robust” array designs, i.e. the Maximum Performance, Maximum Engine Stability, and Maximum HCF Life Expectancy mission designs, are shown in Figures (18) through (20) for both the set of three optimal micro-vane designs and the set of three optimal micro-jet array designs. Optimal micro-jet arrays were examined in Anderson, Miller, Addington, and Agrell<sup>(15)</sup> and the summary performance presented in this report for comparison with the optimal micro-vane designs. These figures also include the baseline inlet performance, i.e. the performance of the redesigned M2129 inlet S-duct without flow control. The low strength effector units used in these designs achieved a substantial improvement in inlet total pressure recovery (PFAVE) over the baseline performance. See Figure (18). This differs from the performance of the high strength effector units which never increased the inlet total pressure recovery above the baseline value<sup>(5)</sup>. A comparison between the set of three (3) optimal micro-jet arrays and the set of three (3) optimal micro-vane arrays indicates a substantial increase in total pressure recovery as a result of using micro-jet arrays. See Figures (18a) and (18b). However, care must be taken about making judgements about the impact of micro-vane vs. micro-jets. The penalties associated with bleeding high pressure engine flow to increase total pressure recovery must be evaluated through a complete vehicle system study to determine the overall systems benefit or penalty.

Excellent engine face distortion characteristics were also achieved with the micro-effector units, i.e both micro-jet and micro-vanes, as shown in Figure (19). Essentially no performance differences were evident between micro-vanes and micro-jet arrays with regards to engine face distortion. See Figures (19a) and (19b).

Presented in Figure (20) is a comparison of the first five Fourier harmonic 1/2-amplitudes for the set of three (3) optimal designs for both micro-jet and micro-vane arrays. Minimizing the mean of the first five Fourier harmonic 1/2-amplitudes resulted in a substantial reduction in the amplitudes of the first three harmonics 1/2-amplitudes, and very low amplitudes for the fourth and fifth harmonic components. Figures (20a) and (20b) include eighteen (18) matched pairs of independent CFD observations for the Fourier harmonic 1/2 amplitude distortion for three (3) optimal array designs arising from three (3) mission strategies. The data has been ordered such that the differences in each of the eighteen (18) matched pairs of CFD observations can be tested as a paired t-test. In a paired t-test, the mean of the sample difference and the standard deviation of the sample difference is calculated and the following t-statistic determined:

$$t^* = \frac{\left| \frac{1}{N} \sum_{j=1}^N \Delta_j \right|}{\sqrt{\sum_{j=1}^n \frac{(\Delta_j - \bar{\Delta})^2}{(N-1)}}} \quad (14)$$

where  $\Delta_j = (Y_1 - Y_2)_j$  is the difference of each of the N-pairs of the response variable in the two data sets.

In the paired t-test, if the expression

$$t^* < t(0.975, v_p) \quad (15)$$

is valid, the response values from the first data set are not statistically different from the response values from the second data set at the 95% confidence level. Conversely, the response values from the first data set are statistically different from the response values from the second data set at the 95% confidence level if the following expression is valid:

$$t^* > t(0.975, v_p) \quad (16)$$

Comparing the set of three (3) Fourier micro-vane harmonic 1/2 amplitude profiles represented by Figure (20a) and the set of three (3) Fourier micro-jet harmonic 1/2 amplitude profiles represented by Figure (20b), the mean of the sample difference  $MEAN = 0.0021$  and the standard deviation of the sample difference  $STDEV = 0.0043$ . This gives a t-static  $t^* = 0.4923$ , which when compared to a t value  $t(0.975, 17) = 2.110$ , indicates there were no statistically significant differences between the two (2) sets of three (3) optimal cases at the 95% confidence level. Even though there are differences between the micro-vane and micro-jet the factor variables that define the optimal array designs, these factor differences did not translate into statistically significant differences in the Fourier harmonic 1/2 amplitudes of distortion. Therefore, no conclusions can be drawn as to the relative merits of optimal micro-vane arrays as compared to optimal micro-jet arrays in managing the Fourier harmonic 1/2 amplitudes of engine face distortion. There are no statistically significant differences.

### Statistical Comparison of CFD Analysis and DOE Predictions

A direct statistical comparison can be made between the optimal responses predicted by the DOE models ( $Y_{DOE}$ ) and the actual CFD predicted performance values ( $Y_{CFD}$ ) through the t-statistic:

$$t^* = \frac{|(Y_{CFD}) - (Y_{DOE})|}{\frac{(Y_A) - (Y_{DOE})}{t(0.975, N - p)}} \quad (17)$$

where  $Y_A$  is the upper 95% confidence interval for the individual predicted response  $Y_{DOE}$  from the regression model, and  $t(0.975, N-p)$  is the 95% confidence t-value for  $N-p$  degrees of freedom. Equation (17) was used for the evaluation of the PFAVE regression model.

When there exist a functional relationship between the mean values and standard deviation of the data, the data do not satisfy the requirement that the variation is normally distributed. This often happens when there is a decade or more variation in the response variables range over the design (DOE) space. Under this condition, a transformation is often used to stabilize the variation over the response variable range. Because this was the case with DC60 and the first five Fourier harmonic 1/2-amplitudes, the natural logarithm of these responses was used in the DOE analysis with the t-statistic defined by:

$$t^* = \frac{|\ln(Y_{CFD}) - \ln(Y_{DOE})|}{\frac{\ln(Y_A) - \ln(Y_{DOE})}{t(0.975, N - p)}} \quad (18)$$

Equation (18) was used in the evaluation of the (DC60) and the five Fourier harmonic 1/2-amplitude (F1/2, F2/2, F3/2, F4/2, F5/2) regression models.

For a statistically significant difference to exist between the DOE model predicted response ( $Y_{DOE}$ ) and the CFD validation response prediction ( $Y_{CFD}$ ), the expression:

$$t^* > t(0.975, N - p) \quad (19)$$

must hold. Likewise, if the expression

$$t^* < t(0.975, N - p) \quad (20)$$

is valid, the  $Y_{CFD}$  is not statistically different from  $Y_{DOE}$ . Therefore, for no significant statistical difference to exist between the DOE model predicted response  $Y_{DOE}$  and the CFD analysis response  $Y_{CFD}$ , the CFD response prediction must fall within the 95% confidence interval of the

DOE model prediction for that response. For each “Optimal Robust” array design, the statistical comparisons were made between the corresponding responses for the cases in each set listed in Tables (10) and (11).

Table (12) presents the results of a statistical comparison between the CFD analysis and DOE predictions for the Maximum Performance, Maximum Engine Stability, and Maximum HCF Life Expectancy missions for the eight (8) response parameters. The eight response parameters include the inlet total pressure (PFAVE), the engine face distortion (DC60), the first five Fourier harmonic 1/2 amplitudes of distortion (F1/2, F2/2, F3/2, F4/2, F5/2), and the mean of the first five Fourier harmonic 1/2 amplitudes of distortion (FM/2). With the exception of two (2) cases, the comparisons indicate that the DOE prediction results are not statistically different from the CFD analysis. These CFD analysis predictions fell within the 95% confidence interval of the DOE performance predictions generated from the DOE response surfaces. However, for those two cases in which a statistical difference were indicated, the actual differences between the CFD analysis and DOE prediction were small relative to experimental error. Therefore, the optimal arrays determined by the DOE regression models were a statistically valid optima when compared to the actual CFD array analyses. The accuracy of the response surfaces determined from the DOE prediction was therefore sufficient for determining optimal array designs.

## CONCLUSIONS

The fundamental importance of *Response Surface Methods* over traditional design approaches lies in the optimal sequenced pattern of Design-of-Experiments (DOE), the statistical model building, and the systematic procedures for the optimization of design configurations. *Response Surface Methods* allows the number of CFD cases run to be optimized, depending on the program objectives, for a substantial reduction in the number of CFD experiments to be run. RSM also provides an economical, reliable and systematic approach to variable screening as well as the general exploration of the region that contains the estimated optimal conditions. As a result, the pragmatic use of RSM places a high priority on obtaining a better understanding of the process system as well as estimating the optimum conditions. In the design of microscale secondary flow arrays for compact inlets, it is just as important to understand and quantify the behavior of the factor (design) parameters in the neighborhood of the optimal conditions as knowing the optimal conditions. Hence, an RSM approach is particularly beneficial for the design of micro-vane arrays since there are a great many factor (design) variables available to the aerodynamicist, and often there exists multiple design objectives. Also multiple mission optimal arrays were determined with *Response Surface Methods* without repeating the optimization procedure.

The use of micro-vane actuation in the revised M2129 S-duct was dominated by the two-factor interactions ( $n^*h$ ) and ( $h^*c$ ) for inlet total pressure recovery (PFAVE) and three two-factor interactions ( $n^*h$ ), ( $n^*c$ ) and ( $h^*c$ ) for engine face (DC60) distortion. Without objective information about these two-factor interactions, optimal micro-vane array designs can not be determined. In general, the optimal use of micro-vane actuation in the revised M2129 S-duct was very effective in simultaneously managing the inlet total pressure recovery, engine face distortion and the Fourier harmonic 1/2 amplitude content of engine face distortion.

To illustrate the potential of *Response Surface Methods*, three different mission strategies were considered for the subject inlet, namely (1) Maximum Performance, (2) Maximum Engine Stability, and (3) Maximum HCF Life Expectancy. The Maximum Performance mission minimized the inlet total pressure losses, the Maximum Engine Stability mission minimized the

engine face distortion (DC60), while the Maximum HCF Life Expectancy mission minimized the mean of the first five Fourier harmonic amplitudes, i.e. “collectively” reduced all the harmonic 1/2-amplitudes of engine face distortion. By visually comparing the CFD validation performance of the three optimal arrays designs, i.e. Maximum Performance, Maximum Engine Stability, and the Maximum HCF Life Expectancy, it is obvious that they are remarkably similar. Also, a visual comparison between the performance of the three optimal arrays designs determined by the DOE prediction and the CFD validation analysis shows remarkable similarity. A comparison between optimal arrays determined by the DOE prediction and CFD analysis indicates statistically differences occurred about 8% of the time, which is remarkably good. All the cases in which a statistical difference were indicated involved the evaluation of the Fourier harmonic 1/2-amplitudes of distortion. In these particular cases, the differences between the CFD analysis and DOE prediction were too small to be of practical significance, i.e. they could not be experimentally measured. This indicates that the DOE prediction results were not statistically different from the CFD analysis results (i.e. the CFD analysis predictions fell within the 95% confidence interval of the DOE performance predictions). It also indicated that the optimal arrays determined by the DOE models were a statistically valid optima when compared to the actual CFD array analyses. The accuracy of the response surfaces determined from the DOE analysis was therefore more than adequate for use in determining an array optimum.

A comparison between the set of three (3) optimal micro-jet arrays and the set of three (3) optimal micro-vane arrays indicates a substantial increase in total pressure recovery as a result of the using micro-jet arrays. However, care must be taken in making judgments about micro-jets vs. micro-vane as the penalty for bleeding 1.0% engine flow has not been included in this study. Excellent engine face distortion characteristics were also achieved with the micro-effector units, i.e both micro-jet and micro-vanes. Essentially no performance differences were evident between micro-vanes and micro-jet arrays with regards to engine face distortion. A paired t-test comparison between the set of three (3) optimal Fourier micro-vane harmonic 1/2 amplitude profiles and the set of three (3) Fourier micro-jet harmonic 1/2 amplitude profiles indicated no statistical significant differences between the two (2) sets of three (3) optimal cases at the 95% confidence level. Even though there are differences between the micro-vane and micro-jet the factor variables that define the optimal array designs, these factor differences did not translate into statistically significant differences in the Fourier harmonic 1/2 amplitudes of distortion.

## REFERENCES

- (1) Anderson, B. H., Miller, D. N., Yagle, P. J., and Truax, P. P., "A Study of MEMS Flow Control for the Management of Engine Face Distortion in Compact Inlet Systems", FEDSM99-6920, 3rd ASME/JSME Joint Fluids Engineering Conference, San Francisco, CA, July 18-23, 1999.
- (2) Hamstra, J. W., Miller, D. N., Truax, P. P., Anderson, B. H., and Wendt, B. J., "Active Inlet Flow Control Technology Demonstration," ICAS-2000-6.11.2, 22nd International Congress of the Aeronautical Sciences, Harrogate, UK, August 27th-September 1st, 2000.
- (3) Box, G. E. P., and Jones, S., "*Empirical Model Building and Response Surfaces*," John Wiley, New York, 1987
- (4) Box, G. E. P., Hunter, W. G., and Hunter, J. S., "*Statistics for Experimenters*," John Wiley, New York, 1978.
- (5) Anderson, B. H., Baust, H. D., and Agrell, J., "Management of Total Pressure Recovery, Distortion, and High Cycle Fatigue in Compact Air Vehicle Inlets," NASA/TM-2002-212000, Dec. 2002.
- (6) AGARD FTP Working Group 13, "Air Intakes for High Speed Vehicles", AR-270, September 1991.
- (7) Willmer, A. C., Brown, T. W. and Goldsmith, E. L., "Effects of Intake Geometry on Circular Pitot Intake Performance at Zero and Low Forward Speeds", Aerodynamics of Power Plant Installation, AGARD CP301, Paper 5, Toulouse, France, May 1981, pp 51-56.
- (8) Anderson, B. H. and Keller, D. J., "Optimal Micro-Scale Secondary Flow Control for the Management of HCF and Distortion in Compact Inlet Diffusers", NASA/TM-2002-211686, July 2002.
- (9) Anderson, B. H. and Keller, D. J., "A Robust Design Methodology for Optimal Micro-Scale secondary Flow Control in Compact Inlet Diffusers", AIAA Paper No. 2002-0541, Jan. 2002.
- (10) Anderson, B. H. and Keller, D. J., "Robust Design Methodologies for Optimal Micro-Scale Secondary Flow Control in Compact Inlet Diffusers", NASA/TM-2001-211477, March 2001.
- (11) Bender, E. E., Anderson, B. H., and Yagle, P. J., "Vortex Generator Modeling for Navier Stokes Code", FEDSM99-69219, 3rd ASME/JSME Joint Fluids Engineering Conference, San Francisco, CA, July 18-23, 1999.

- (12) Ludwig, G. R., “Aeroelastic Considerations in the Measurement of Inlet Distortion”, 3rd National Turbine Engine High Cycle Fatigue Conference, 1998.
- (13) Anderson, B. H. and Keller, D. J., “Considerations in the Measurements of Engine Face Distortion for High Cycle Fatigue in Compact Inlet Diffusers”, NASA/M-2001-211476, March 2001.
- (14) Goldsmith, E. L., and Seddon, J. (eds), “*Practical Intake Aerodynamics*,” Blackwell Scientific Publications, Oxford, 1993.
- (15) Anderson, B. H., Miller, D. N., Addington, G. A., and Agrell, J., “Optimal Micro-Jet Flow Control for Compact Air Vehicle Inlets,” Proposed NASA/TM, 2003.

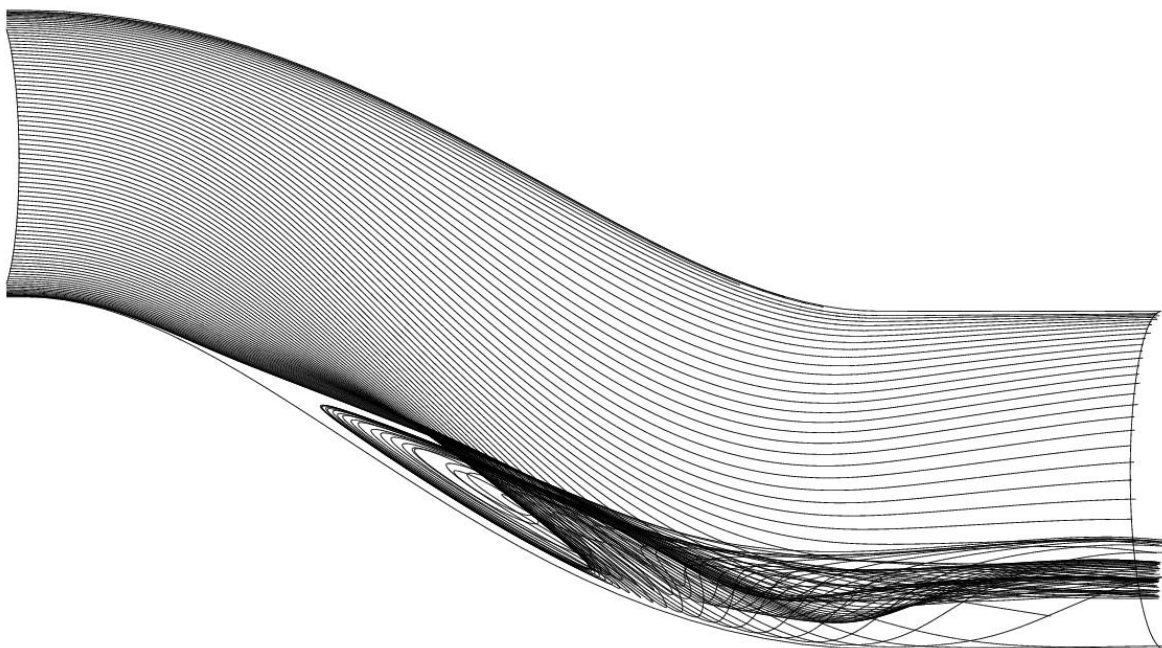
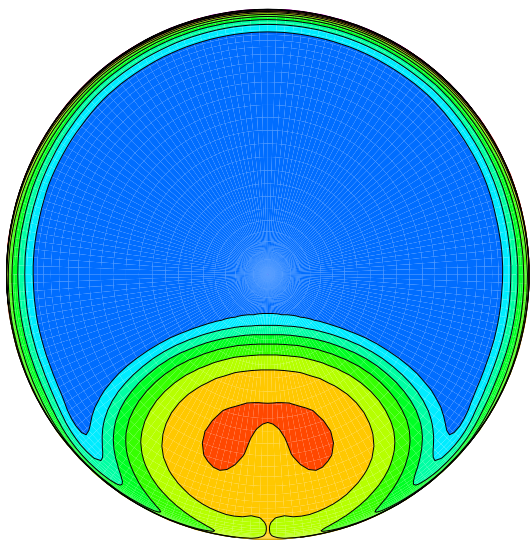
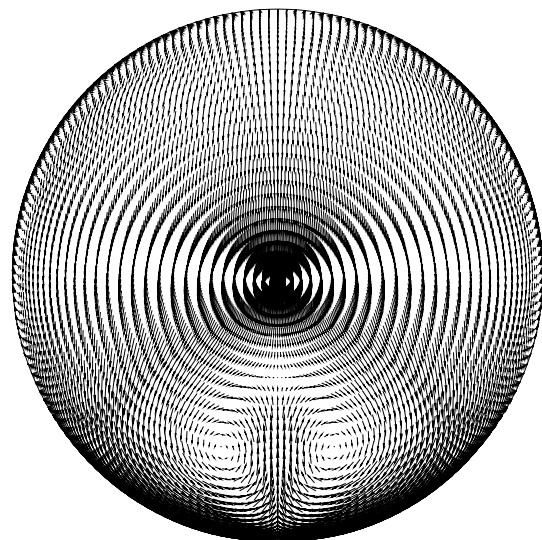


**Figure (1): Near wall streamlines in baseline inlet S-duct,  $Mt = 0.70$ ,  $\alpha = 0.0$  (deg).**



**(a) Total Pressure Recovery Contours**



**(b) Secondary Velocity Vectors**

**Figure (2): Engine face flow field in baseline inlet S-duct,  $Mt = 0.70$ ,  $\alpha = 0.0$  (deg).**

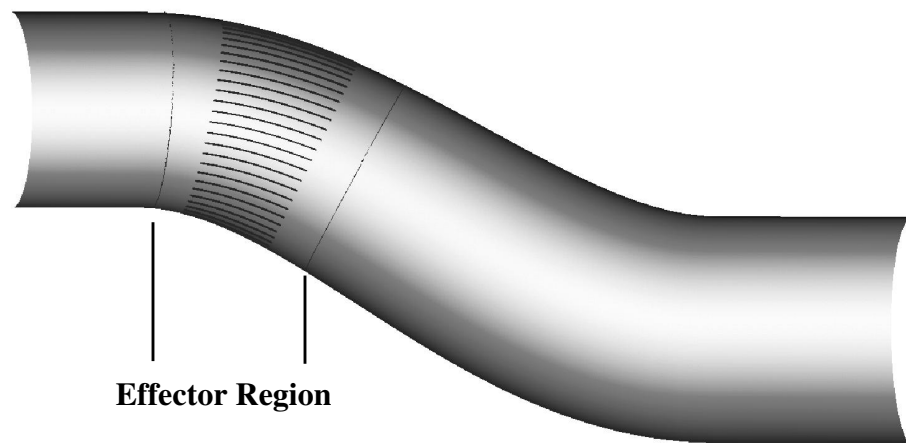


**Figure (3) Location of effector region within inlet S-duct configuration.**

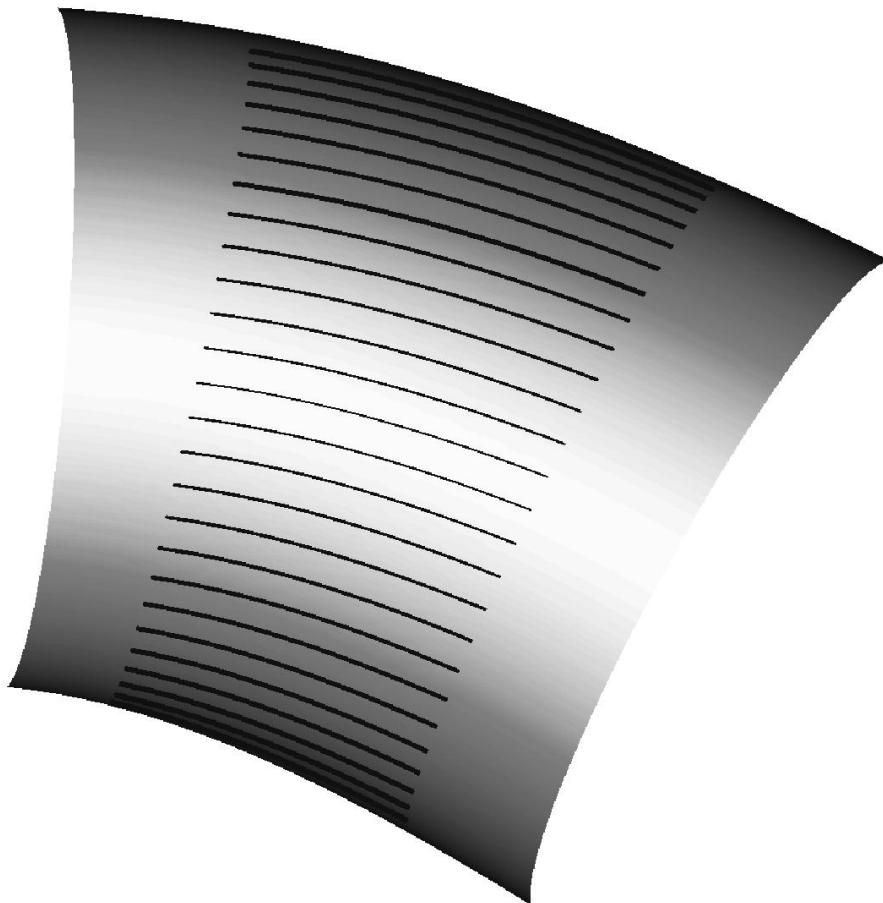


**Figure (4); Micro-vane atonement within inlet S-duct effector region.**

Factor	Range
Number of Micro-Vane Effectors, n	13 to 27
Micro-Vane Effector Height (mm), h	1.0 to 2.0
Micro-Vane Effector Chord Length (mm), c	36.0 to 72.0

**Table (1): Factor variables which establish the DOE design matrix.**

Variable	Value
Effector Vane Thickness (mm), t	0.138
Micro-Vane Effector Angle-of-Incidence (deg), $\beta$	5.0
Inlet Total Pressure (lbs/ft <sup>2</sup> ), Pt	10506.0
Inlet Total Temperature (°R), Tt	517.0
Inlet Throat Mach Number, Mt	0.70
Inlet Angle-of-Incidence (deg), $\alpha$	0.0
Inlet Angle-of-Yaw (deg), $\gamma$	0.0

**Table (2): Variables held constant.**

Response	Nomenclature
Engine Face Total Pressure Recovery	PFAVE
Engine Face Distortion	DC60
1st Fourier Harmonic 1/2 Amplitude	F1/2
2nd Fourier Harmonic 1/2 Amplitude	F2/2
3rd Fourier Harmonic 1/2 Amplitude	F3/2
4th Fourier Harmonic 1/2 Amplitude	F4/2
5th Fourier Harmonic 1/2 Amplitude	F5/2

**Table (3): DOE response variables.**

Config.	n	h	c
nvg601	13	1.0	36.0
nvg602	27	1.0	36.0
nvg603	13	2.0	36.0
nvg604	27	2.0	36.0
nvg605	13	1.0	72.0
nvg606	27	1.0	72.0
nvg607	13	2.0	72.0
nvg608	27	2.0	72.0
nvg615	13	1.5	54.0
nvg615	27	1.5	54.0
nvg615	20	1.0	54.0
nvg615	20	2.0	54.0
nvg615	20	1.5	36.0
nvg615	20	1.5	72.0
nvg615	20	1.5	54.0

**Table (4): Central Composite Face-Centered (CCF) DOE format.**

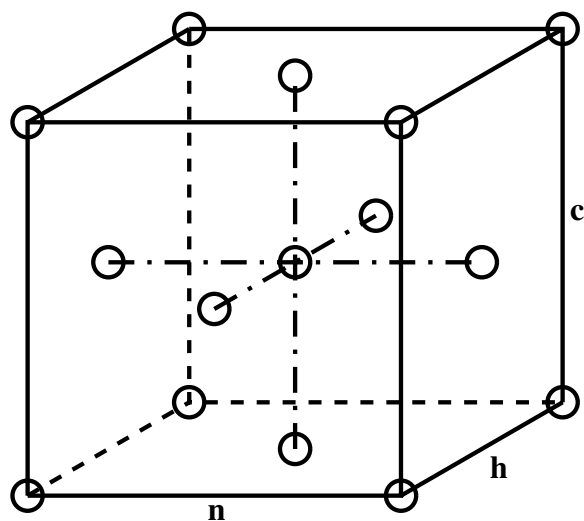
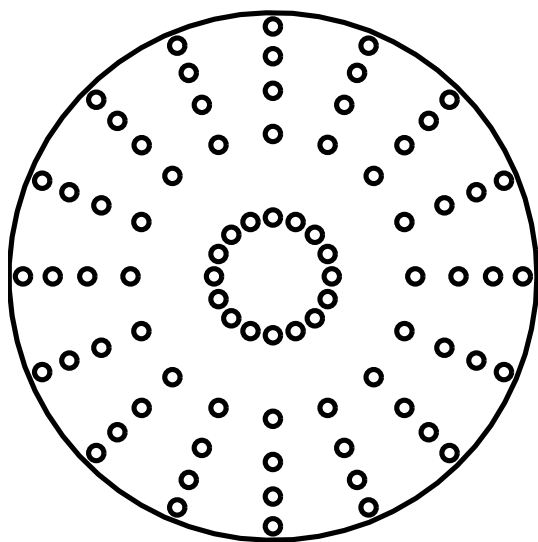


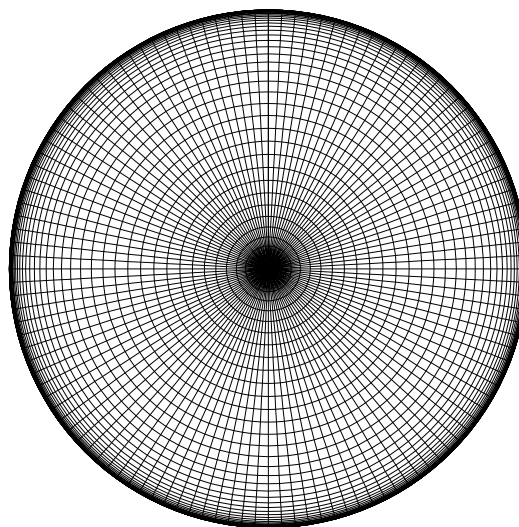
**Figure (5): Graphical representation of the Central Composite Face-Centered (CCF) DOE format.**

Ring Number	Radial Weighting Coefficient
1	0.05651
2	0.14248
3	0.21077
4	0.26918
5	0.32106

**Table (5): Radial weighting coefficients applied to the total pressure rake measurements.**



**(a) 80-probe rake**



**(b) Computational grid**

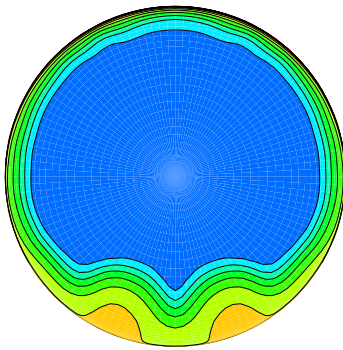
**Figure (6): Total pressure and distortion measurement arrays.**

Response	Nomenclature	$S^2_{\max}/S^2_{\min}$	F(0.975,9,9)
1st Harmonic 1/2 Amplitude	F1/2	2812.8	4.03
2nd Harmonic 1/2 Amplitude	F2/2	309.89	4.03
3rd Harmonic 1/2 Amplitude	F3/2	1718.3	4.03
4th Harmonic 1/2 Amplitude	F4/2	62.128	4.03
5th Harmonic 1/2 Amplitude	F5/2	85.952	4.03

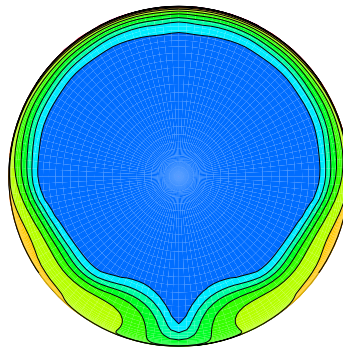
**Table (6): Fourier harmonic 1/2 amplitude F-test compliance**

Config.	PFAVE	DC(60)	F1/2	F2/2	F3/2	F4/2	F5/2
nvg601	0.97405	0.19080	0.01753	0.01474	0.00622	0.00085	0.00368
nvg602	0.97528	0.06825	0.00956	0.00083	0.00744	0.00591	0.00252
nvg603	0.97727	0.03469	0.00278	0.00327	0.00466	0.00345	0.00301
nvg604	0.97633	0.04567	0.00412	0.01193	0.00858	0.00240	0.00339
nvg605	0.97576	0.07640	0.01066	0.00427	0.00234	0.00399	0.00227
nvg606	0.97727	0.05010	0.00034	0.00910	0.01055	0.00332	0.00121
nvg607	0.97850	0.02916	0.00492	0.00842	0.00572	0.00352	0.00288
nvg608	0.97756	0.04964	0.01073	0.01266	0.00578	0.00051	0.00293
nvg609	0.97689	0.03778	0.00414	0.00274	0.00442	0.03050	0.00270
nvg610	0.97680	0.04617	0.00335	0.01119	0.00878	0.00145	0.00209
nvg611	0.97547	0.06399	0.00851	0.00092	0.00770	0.00555	0.00219
nvg612	0.97736	0.03665	0.00517	0.01025	0.00622	0.00231	0.00373
nvg613	0.97614	0.04611	0.00516	0.00374	0.00666	0.00343	0.00270
nvg614	0.97765	0.04418	0.00552	0.01160	0.00700	0.00093	0.00231
nvg615	0.97699	0.04468	0.00277	0.01095	0.00823	0.00159	0.00117

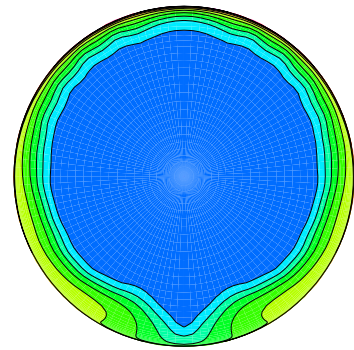
**Table (7): Engine face performance results for the Central Composite Face-Centered (CCF) DOE format.**



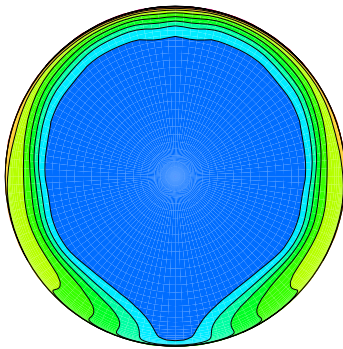
**Config. nvg601**



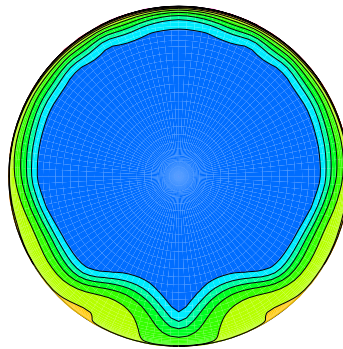
**Config. nvg602**



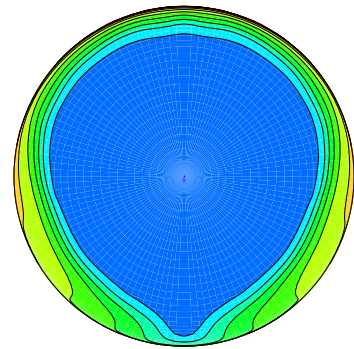
**Config. nvg603**



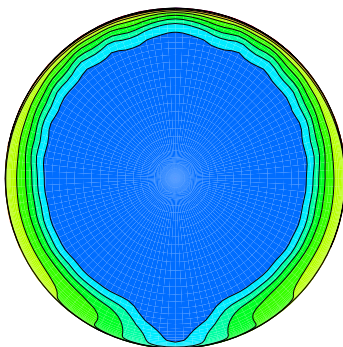
**Config. nvg604**



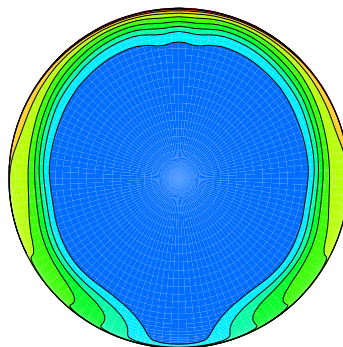
**Config. nvg605**



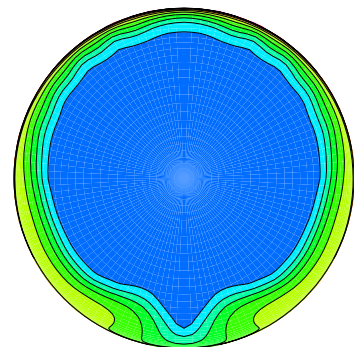
**Config. nvg606**



**Config. nvg607**

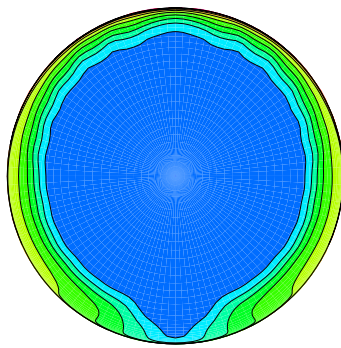


**Config. nvg608**

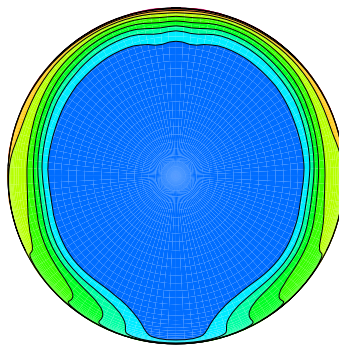


**Config. nvg609**

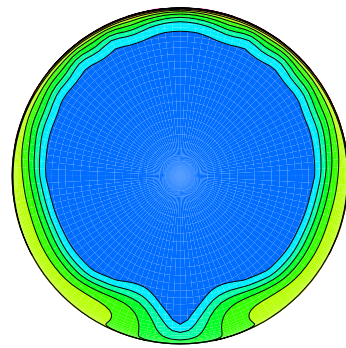
**Figure (7): Engine face total pressure recovery contours for the Central Composite Face-Centered (CCF) Design-of-Experiments matrix.**



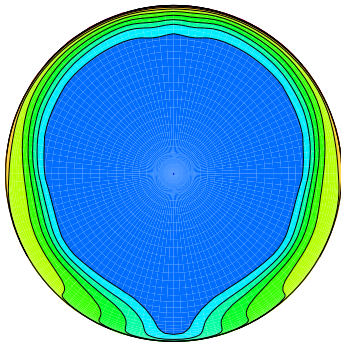
**Config. nvg607**



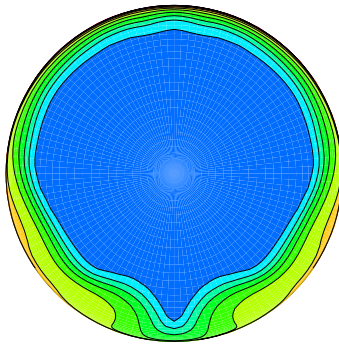
**Config. nvg608**



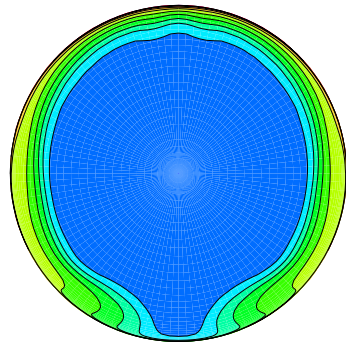
**Config. nvg609**



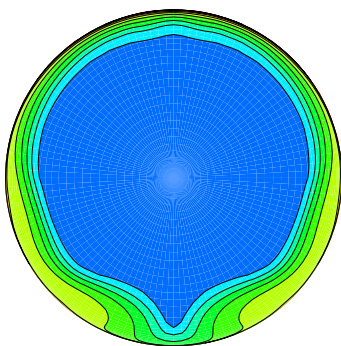
**Config. nvg610**



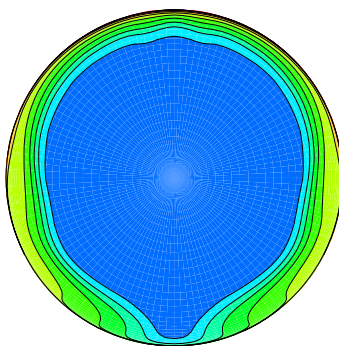
**Config. nvg611**



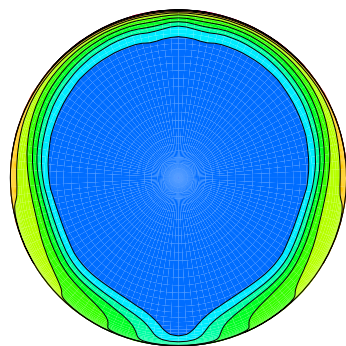
**Config. nvg612**



**Config. nvg613**



**Config. nvg614**



**Config. nvg615**

**Figure (7): Engine face total pressure recovery contours for the Central Composite Face-Centered (CCF) Design-of-Experiments matrix, concluded.**

Term	Transf. Coeff.	p	% Signif.
1	0.976982	0.0001	99.99
h	0.000893	0.0001	99.99
c	0.000827	0.0001	99.99
n*h	-0.000577	0.0001	99.99
h*c	-0.000186	0.0310	96.90
h <sup>2</sup>	-0.000481	0.0036	99.64

**Table (8): Significance of regression terms in DOE model for inlet total pressure recovery, PFAVE.**

Term	Transf. Coeff.	p	% Signif.
1	-3.176549	0.0001	99.99
h	-0.362611	0.0001	99.99
c	-0.159043	0.0074	99.25
n*h	0.282125	0.0005	99.95
n*c	0.107887	0.0617	93.83
h*c	0.143028	0.0191	98.09
h <sup>2</sup>	0.281190	0.0089	99.99

**Table (9): Significance of regression terms in DOE model for engine face distortion, DC60.**

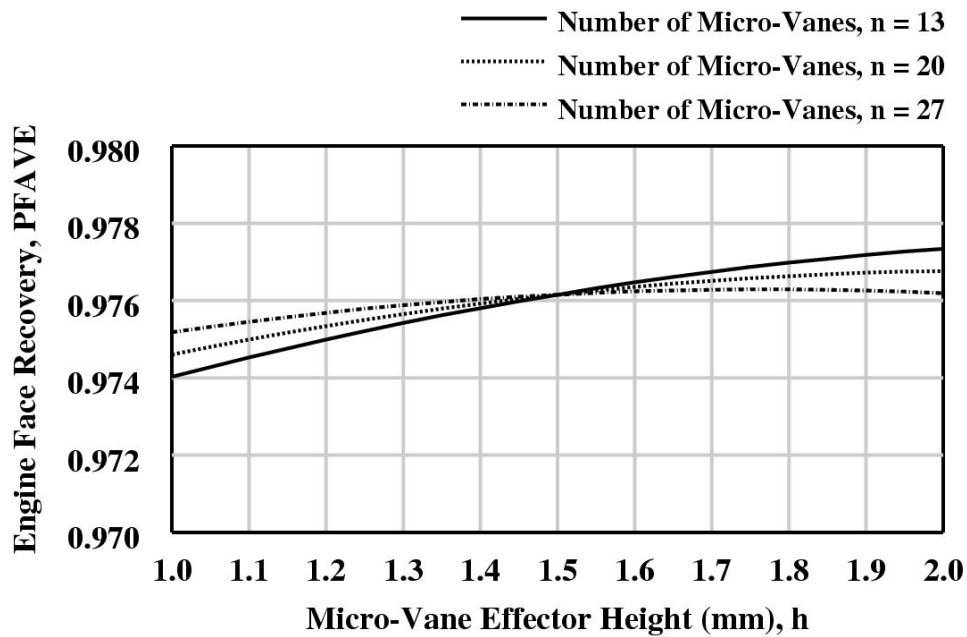


Figure (8): Effect of the micro-vane ( $n \cdot h$ ) interaction on inlet total pressure recovery (PFAVE),  $c = 72.0$  (mm).

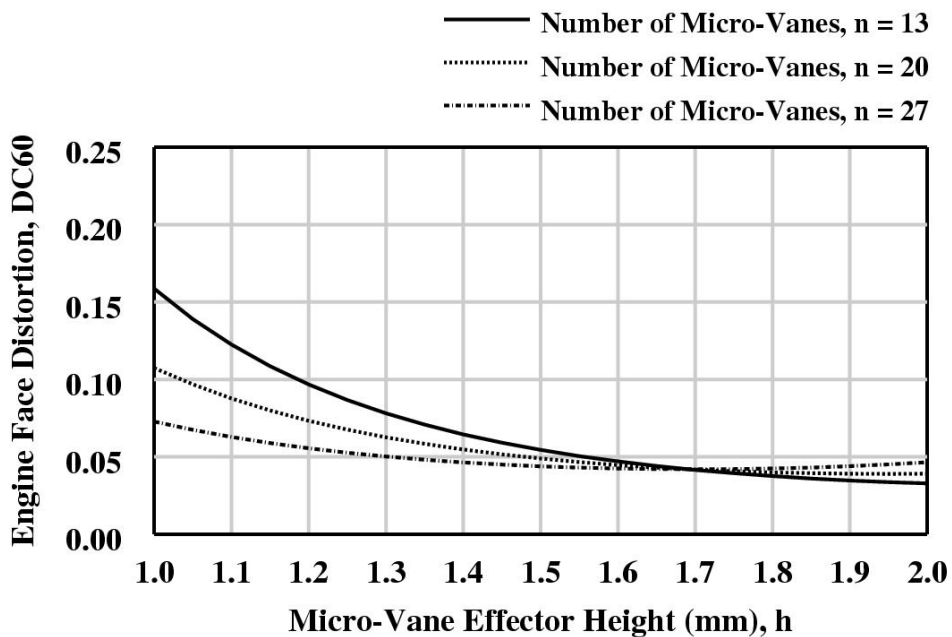


Figure (9): Effect of the micro-vane ( $n \cdot h$ ) interaction on engine face distortion (DC60),  $c = 72.0$  (mm).

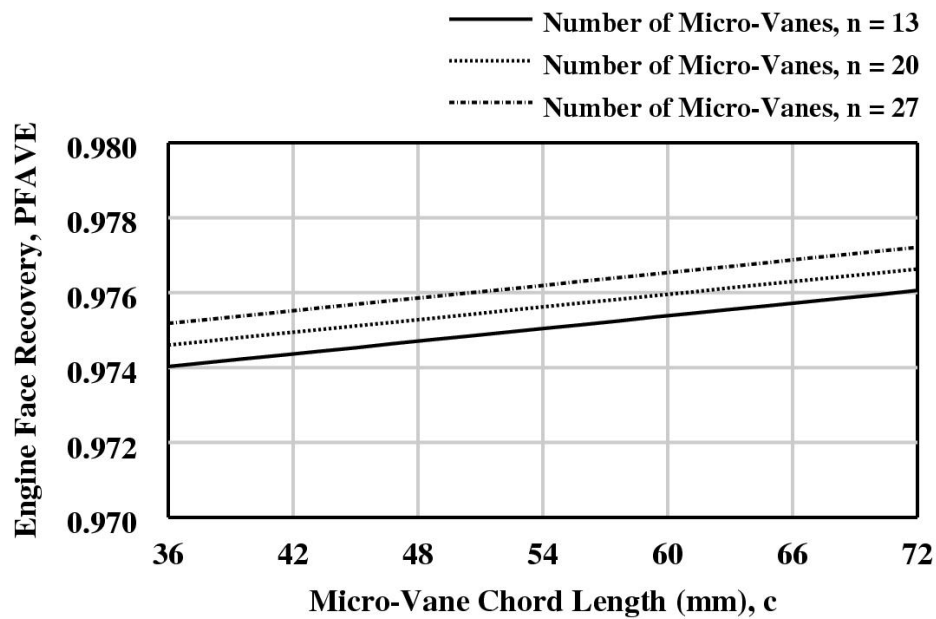


Figure (10): Effect of micro-vane number (n) and chord length (c) on inlet total pressure recovery (PFAVE),  $h = 1.0$  (mm).

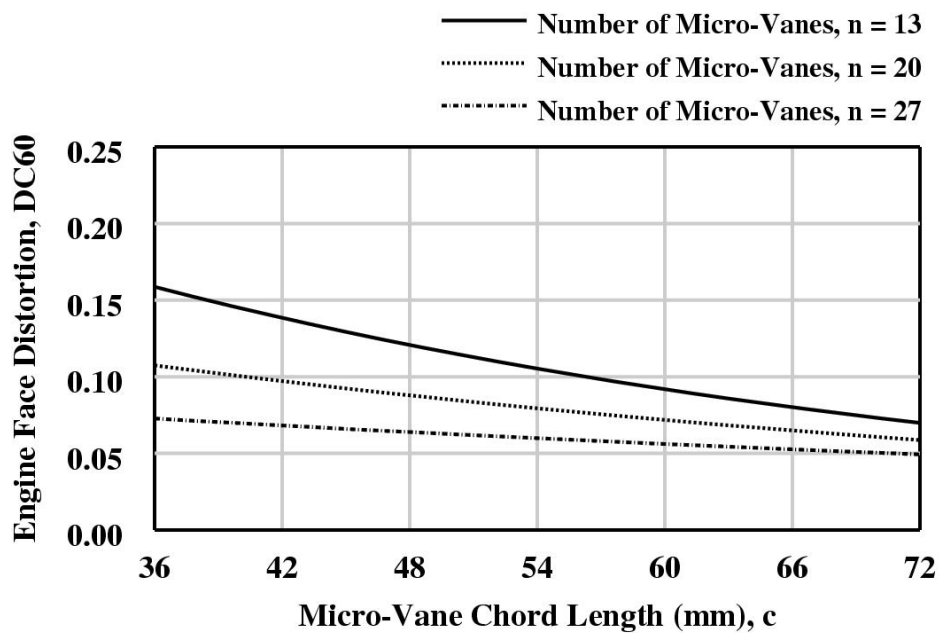
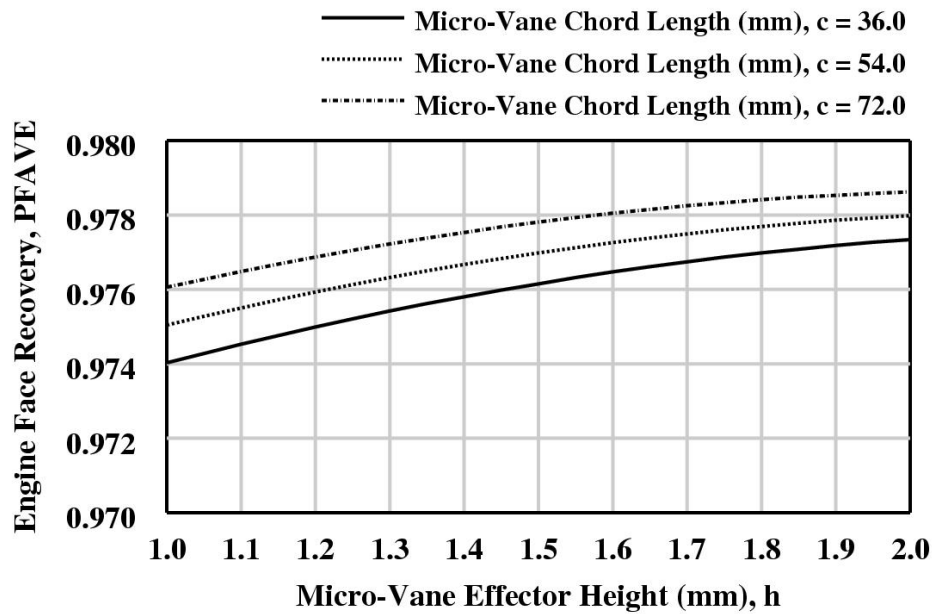
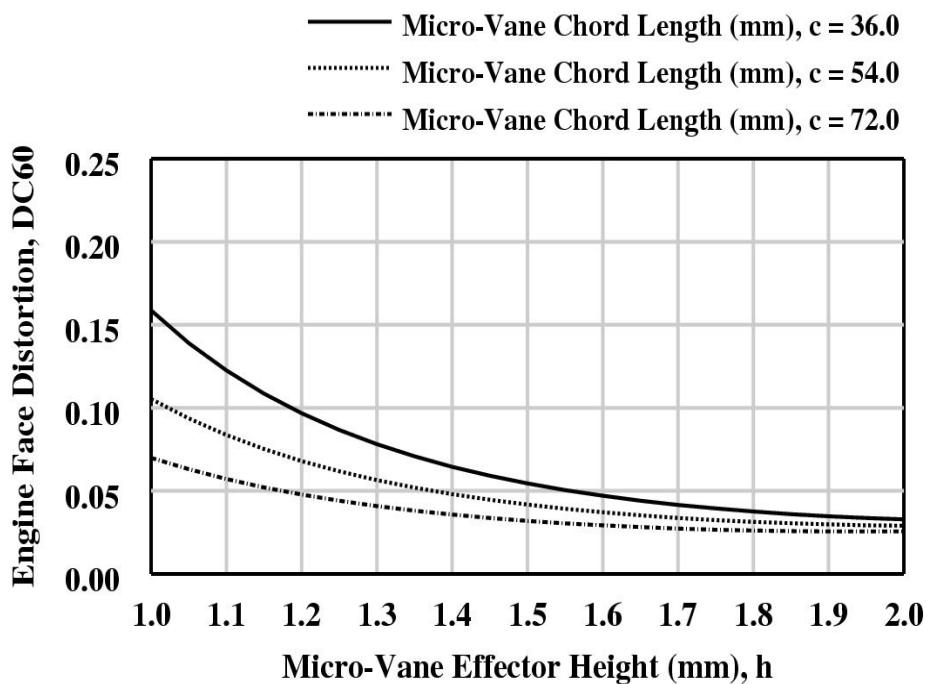


Figure (11): Effect of the micro-vane ( $n \cdot c$ ) interaction on engine face distortion (DC60),  $h = 1.0$  (mm).



**Figure (12):** Effect of the micro-vane ( $h*c$ ) interaction on inlet total pressure recovery (PFAVE),  $n = 13$ .



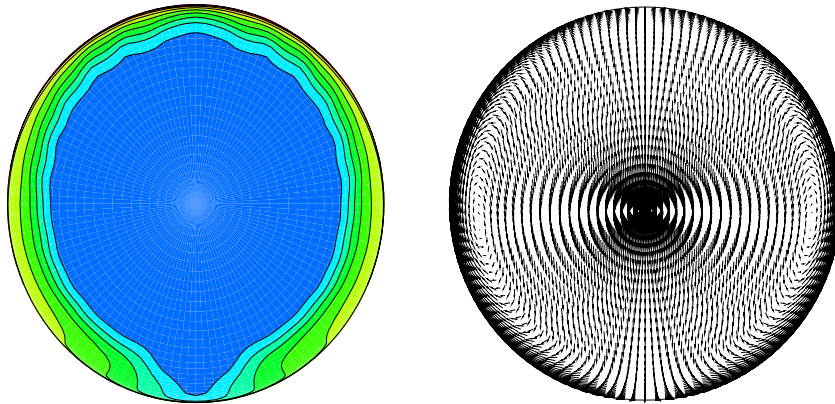
**Figure (13):** Effect of the micro-vane ( $h*c$ ) interaction on engine face distortion (DC60),  $n = 13$ .

Factor/Response	Max. Perf.	Max. Stability	Max. HCF Life
n	13	13	13
h	2.0	1.95	1.55
c	72.0	72.0	72.0
PFAVE	0.97862	0.97858	0.97793
DC60	0.02563	0.02555	0.03048
F1/2	0.00546	0.00511	0.00377
F2/2	0.00422	0.00424	0.00437
F3/2	0.00469	0.00460	0.00420
F4/2	0.00336	0.00328	0.00297
F5/2	0.00139	0.00136	0.00134
FM/2	0.00383	0.00372	0.00333

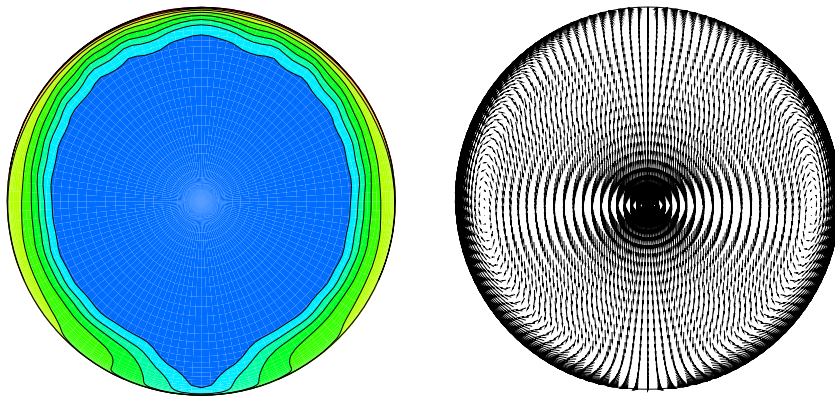
**Table (10): Engine face performance DOE solutions for optimal microscale secondary flow control array designs.**

Factor/Response	Max. Perf.	Max. Stability	Max. HCF Life
n	13	13	13
h	2.0	1.95	1.55
c	72.0	72.0	72.0
PFAVE	0.97850	0.97841	0.97775
DC60	0.02916	0.02867	0.03145
F1/2	0.00492	0.00559	0.00195
F2/2	0.00842	0.00868	0.00818
F3/2	0.00572	0.00491	0.00576
F4/2	0.00352	0.00301	0.00210
F5/2	0.00288	0.00305	0.00185
FM/2	0.00509	0.00501	0.00397

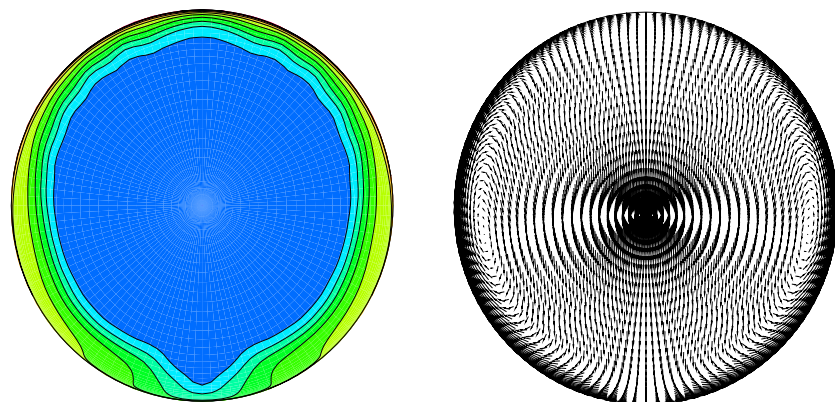
**Table (11): Engine face performance CFD solutions for optimal microscale secondary flow control array designs.**



**(a) Optimal “Maximum Performance” CFD Solution**

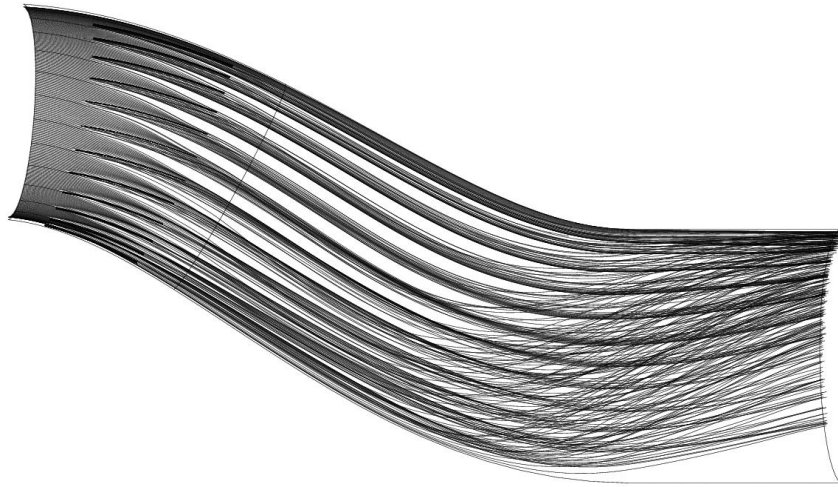


**(b) Optimal “Maximum Engine Stability” CFD Solution**

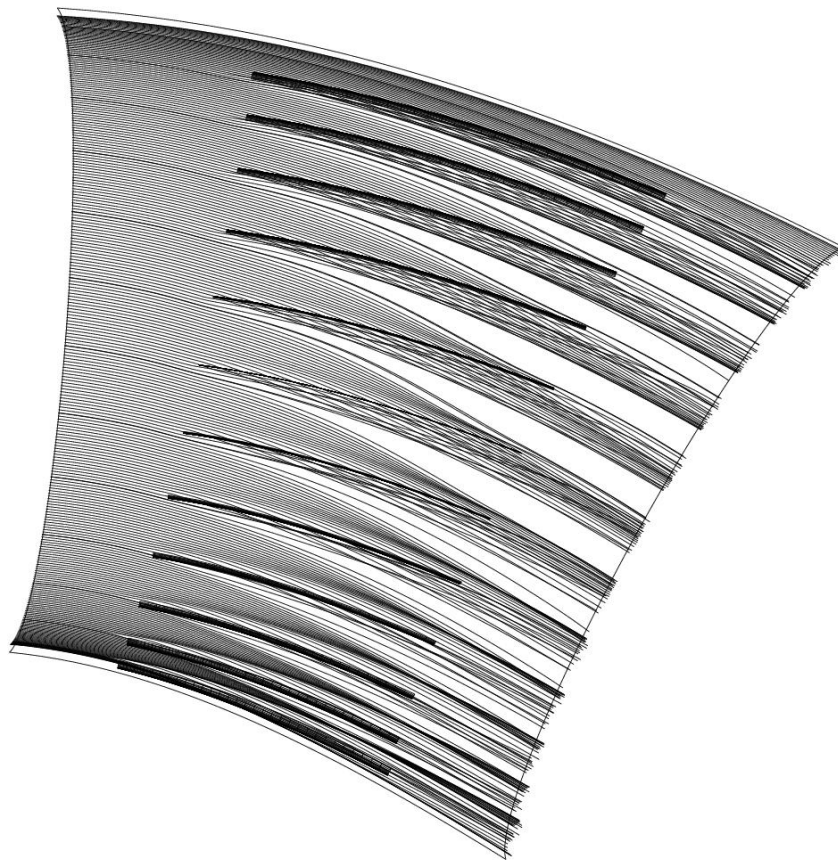


**(c) Optimal “Maximum HCF Life Expectancy” CFD Solution**

**Figure (14): Comparison of total pressure recovery contours for the optimal microscale secondary flow control array CFD solutions,  $Mt = 0.70$ ,  $\alpha = 0.0$  (deg).**

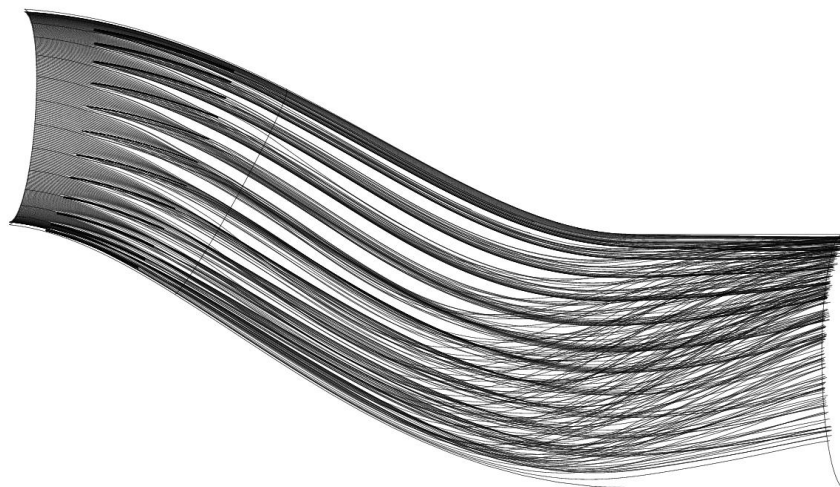


**(a) Inlet near wall streamlines.**

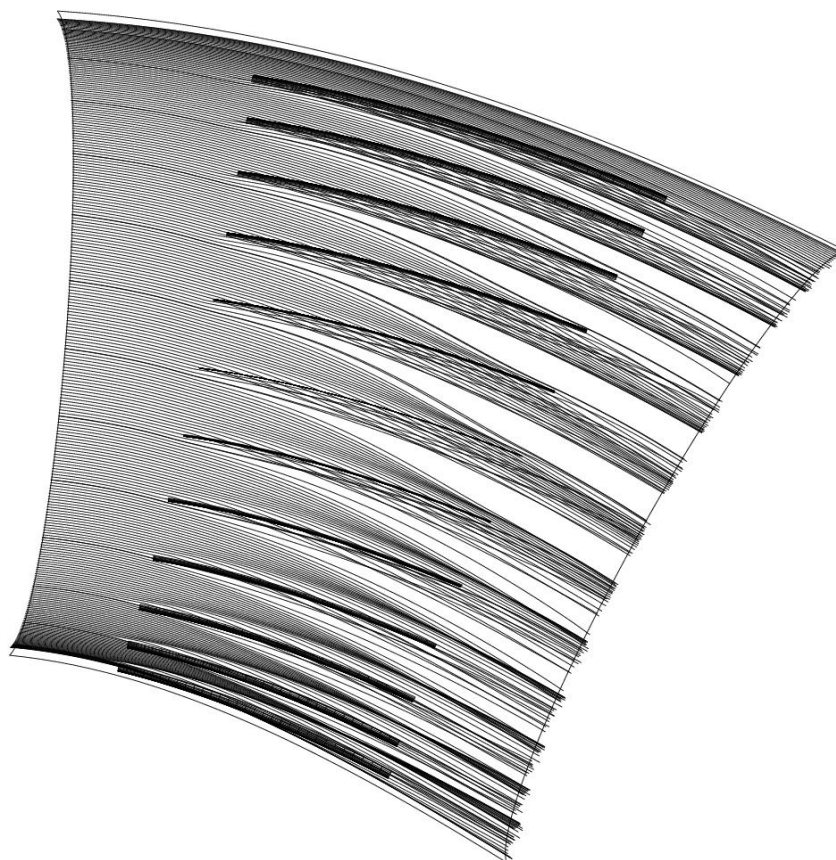


**(b) Effector region near wall streamlines.**

**Figure (15): Near wall streamlines for Optimal Maximum Performance micro-vane array,  $Mt = 0.70$ ,  $\alpha = 0.0$  (deg).**

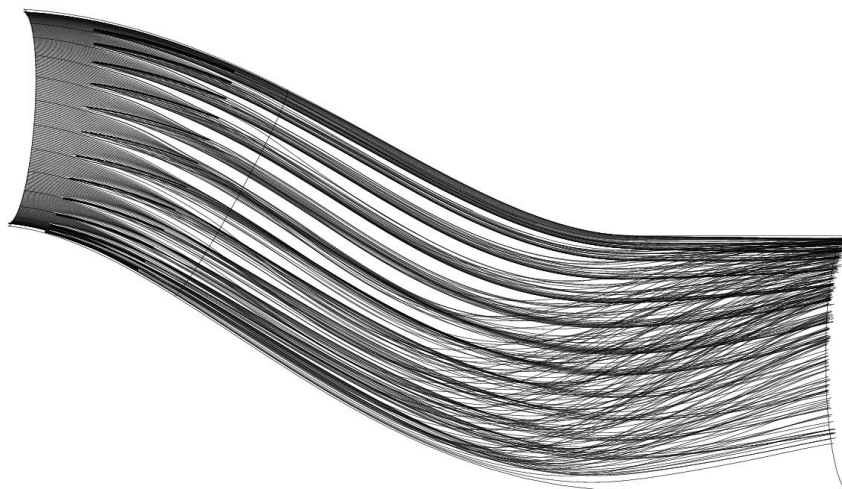


**(a) Inlet near wall streamlines.**

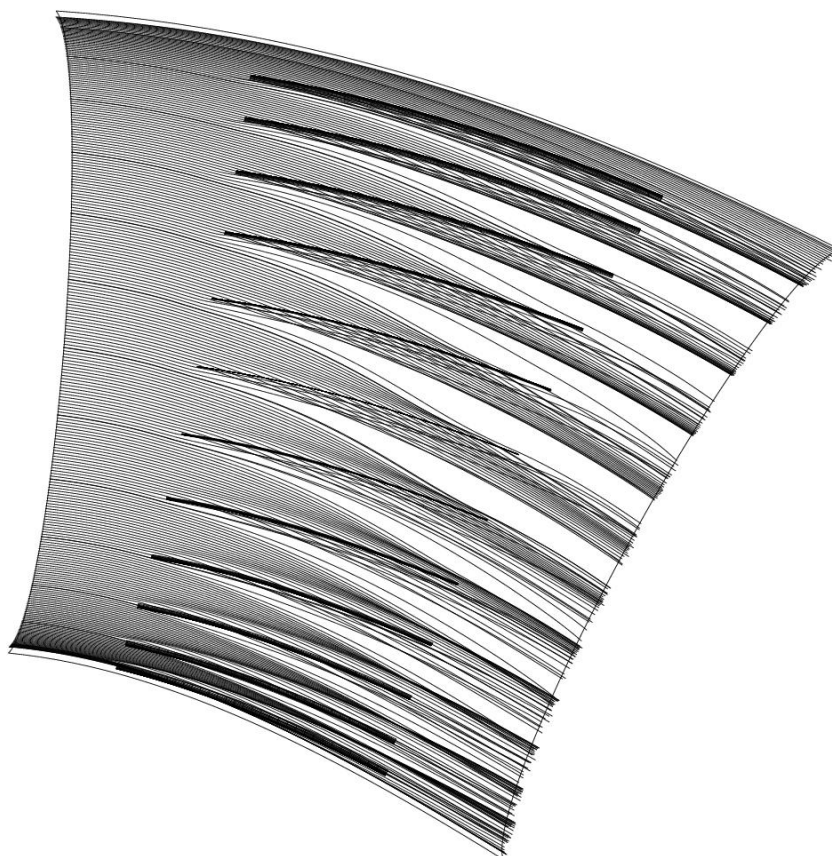


**(b) Effector region near wall streamlines.**

**Figure (16): Near wall streamlines for Optimal Maximum Engine Stability micro-vane array,  $Mt = 0.70$ ,  $\alpha = 0.0$  (degs).**



**(a) Inlet near wall streamlines.**



**(b) Effector region near wall streamlines.**

**Figure (17): Near wall streamlines for Optimal Maximum HCF Life Expectancy micro-vane array,  $Mt = 0.70$ ,  $\alpha = 0.0$  (deg).**

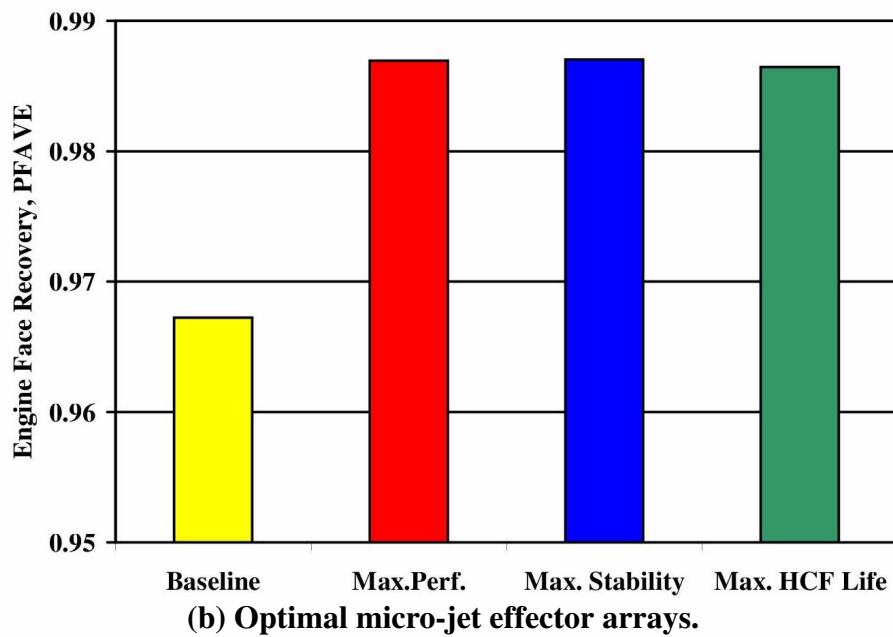
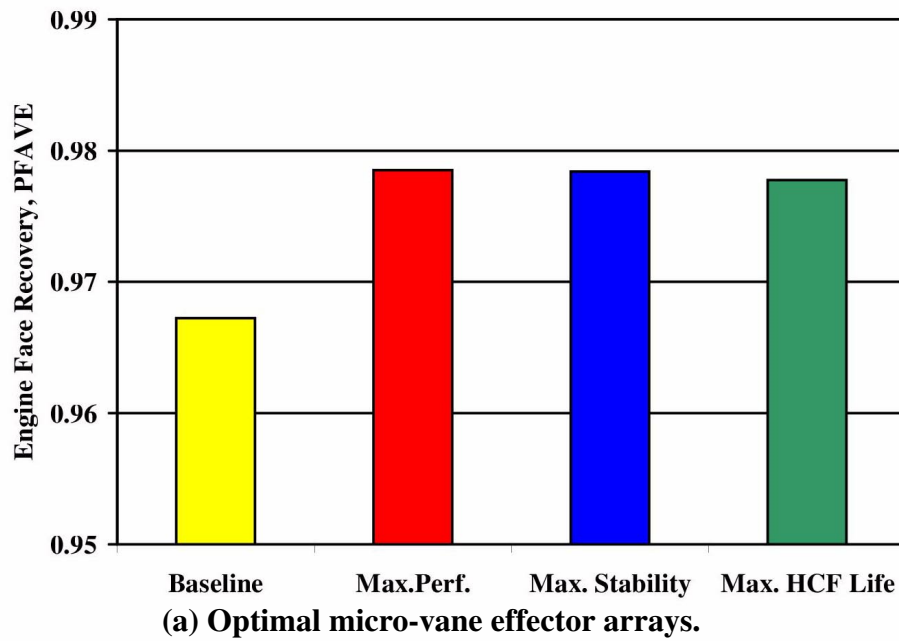
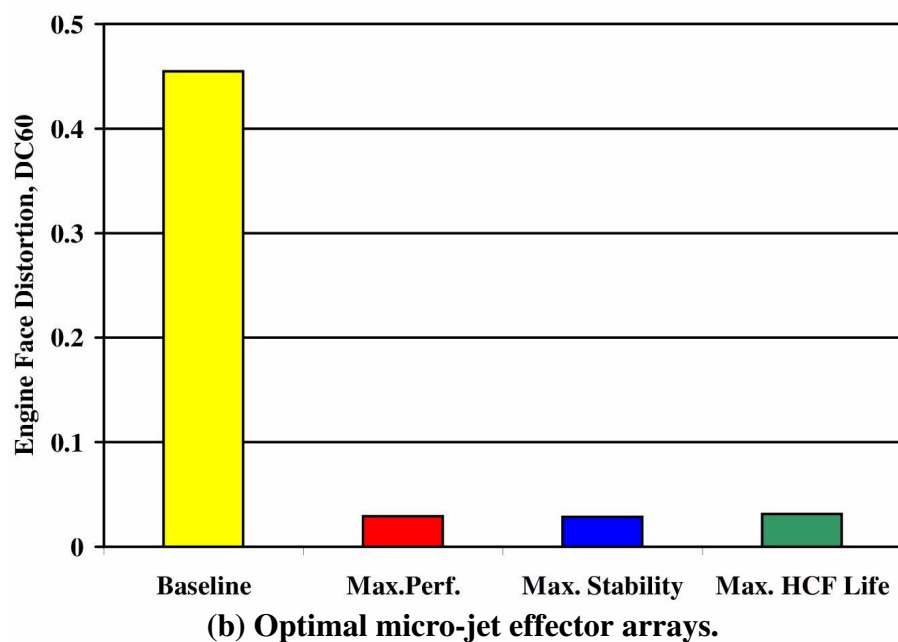
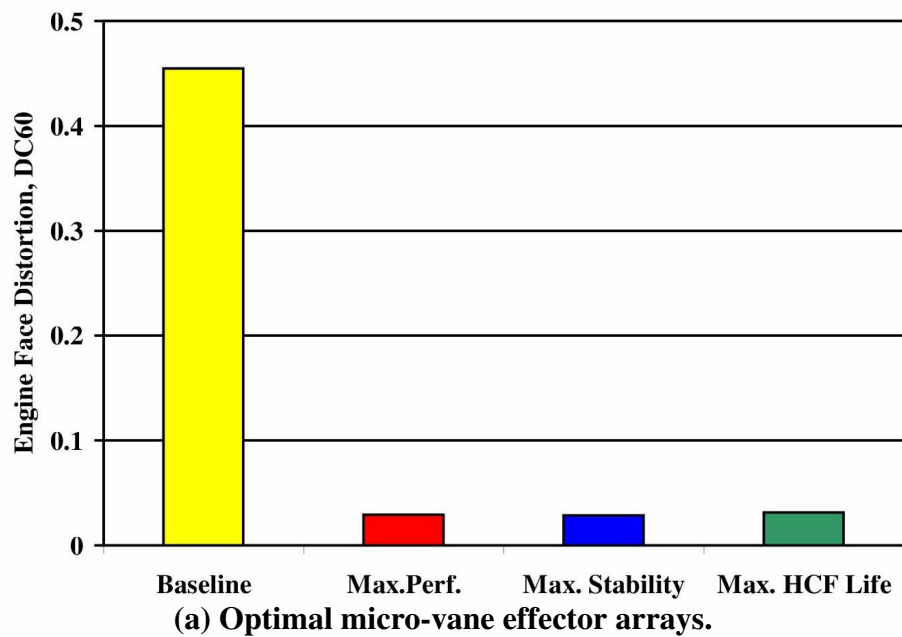
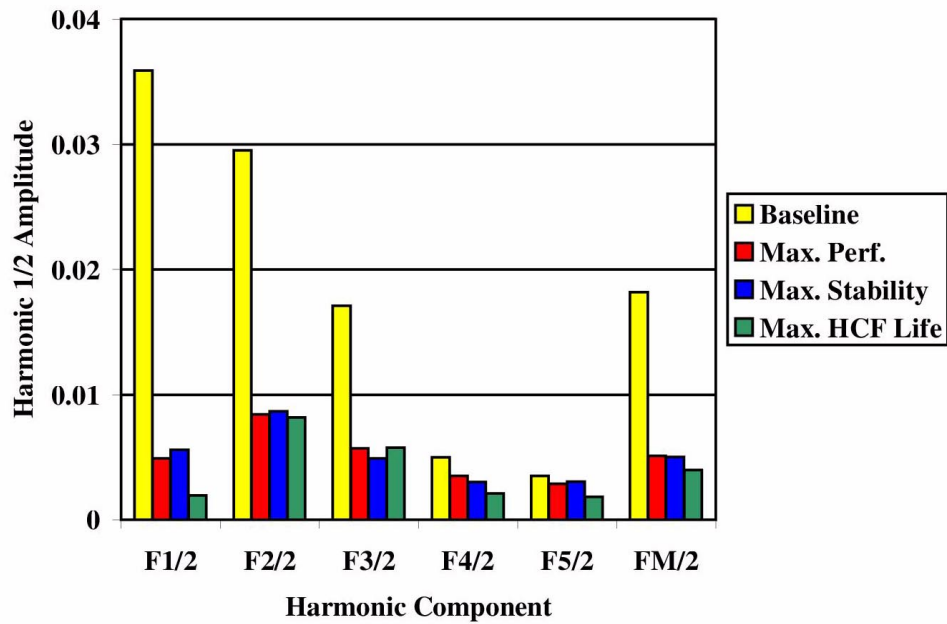


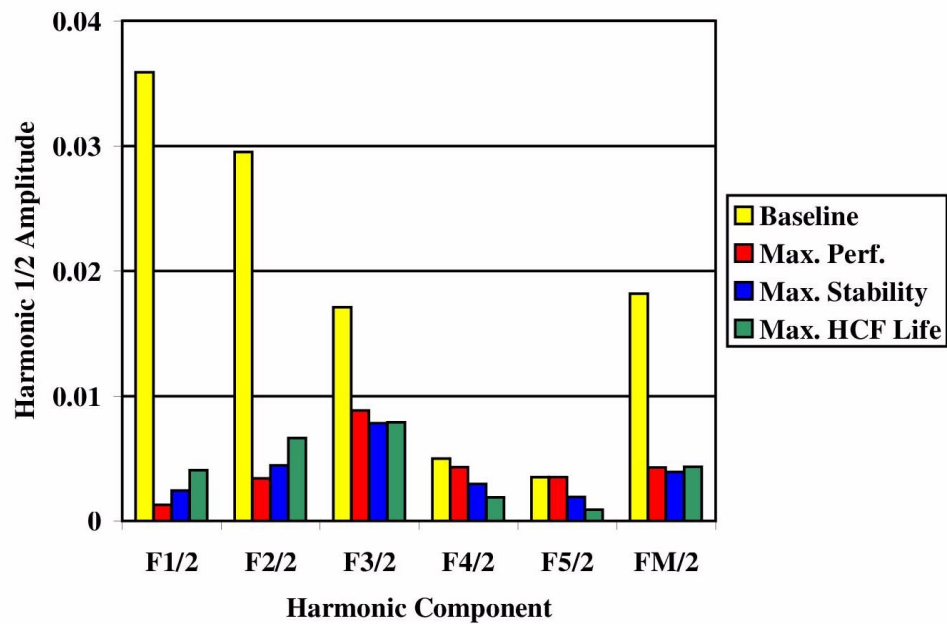
Figure (18): Effect of optimal micro-effector array designs on inlet total pressure recovery (PFAVE),  $M_t = 0.70$ ,  $\alpha = 0.0$  (deg).



**Figure (19): Effect of optimal micro-effector array designs on engine face distortion (DC60),  $M_t = 0.70$ ,  $\alpha = 0.0$  (deg).**



(a) Optimal micro-vane effector arrays.



(a) Optimal micro-jet effector arrays.

Figure (20): Effect of optimal micro-effector array designs on Fourier harmonic 1/2 amplitudes ( $F_k/2$ ),  $M_t = 0.70$ ,  $\alpha = 0.0$  (deg).

Response	Mission	CFD	DOE	t	t*	Comments
PFAVE	Max. Perf.	0.97850	0.97862	2.26216	0.46167	Not Diff.
DC60		0.02916	0.02563	2.30600	0.70669	Not Diff.
F1/2		0.00492	0.00546	1.97681	0.22004	Not Diff.
F2/2		0.00842	0.00422	1.97669	0.95653	Not Diff.
F3/2		0.00572	0.00469	1.97681	2.25177	Diff.
F4/2		0.00352	0.00336	1.97705	0.18062	Not Diff.
F5/2		0.00288	0.00139	1.97635	1.37752	Not Diff.
FM/2		0.00509	0.00383	1.97658	0.98689	Not Diff.
PFAVE	Max. Stability	0.97841	0.97858	2.26216	0.66881	Not Diff.
DC60		0.02867	0.02555	2.30600	0.64757	Not Diff.
F1/2		0.00559	0.00511	1.97681	0.19015	Not Diff.
F2/2		0.00868	0.00424	1.97669	0.99567	Not Diff.
F3/2		0.00491	0.00460	1.97681	0.76783	Not Diff.
F4/2		0.00301	0.00328	1.97705	0.33447	Not Diff.
F5/2		0.00305	0.00136	1.97635	1.53434	Not Diff.
FM/2		0.00501	0.00372	1.97658	1.03429	Not Diff.
PFAVE	Max. HCF Life	0.97775	0.97793	2.26216	0.72842	Not Diff.
DC60		0.03145	0.03048	2.30600	0.18324	Not Diff.
F1/2		0.00195	0.00377	1.97681	1.37152	Not Diff.
F2/2		0.00818	0.00437	1.97669	0.88259	Not Diff.
F3/2		0.00576	0.00420	1.97681	3.85234	Diff.
F4/2		0.00210	0.00297	1.97705	1.31113	Not Diff.
F5/2		0.00185	0.00134	1.97635	0.60891	Not Diff.
FM/2		0.00397	0.00333	1.97658	0.59693	Not Diff.

**Table (12): Statistical comparison between CFD analysis and DOE prediction for the optimal array designs,  $M_t = 0.70$ ,  $\alpha = 0.0$  (degs).**

REPORT DOCUMENTATION PAGE			Form Approved OMB No. 0704-0188	
Public reporting burden for this collection of information is estimated to average 1 hour per response, including the time for reviewing instructions, searching existing data sources, gathering and maintaining the data needed, and completing and reviewing the collection of information. Send comments regarding this burden estimate or any other aspect of this collection of information, including suggestions for reducing this burden, to Washington Headquarters Services, Directorate for Information Operations and Reports, 1215 Jefferson Davis Highway, Suite 1204, Arlington, VA 22202-4302, and to the Office of Management and Budget, Paperwork Reduction Project (0704-0188), Washington, DC 20503.				
1. AGENCY USE ONLY (Leave blank)		2. REPORT DATE February 2004	3. REPORT TYPE AND DATES COVERED Technical Memorandum	
4. TITLE AND SUBTITLE  Optimal Micro-Vane Flow Control for Compact Air Vehicle Inlets			5. FUNDING NUMBERS  WBS-22-708-92-24	
6. AUTHOR(S)  Bernhard H. Anderson, Daniel N. Miller, Gregory A. Addington, and Johan Agrell				
7. PERFORMING ORGANIZATION NAME(S) AND ADDRESS(ES)  National Aeronautics and Space Administration John H. Glenn Research Center at Lewis Field Cleveland, Ohio 44135-3191			8. PERFORMING ORGANIZATION REPORT NUMBER  E-14375	
9. SPONSORING/MONITORING AGENCY NAME(S) AND ADDRESS(ES)  National Aeronautics and Space Administration Washington, DC 20546-0001			10. SPONSORING/MONITORING AGENCY REPORT NUMBER  NASA TM-2004-212936	
11. SUPPLEMENTARY NOTES Bernhard H. Anderson, NASA Glenn Research Center; Daniel N. Miller, Lockheed Martin Aerospace Company, Fort Worth, Texas 76101; Gregory A. Addington, Wright-Patterson Air Force Base, Dayton, Ohio 45433; and Johan Agrell, Swedish Defence Research Agency, Bromma, Sweden SE-17290. Responsible person, Bernhard H. Anderson, organization code 5850, 216-433-5822.				
12a. DISTRIBUTION/AVAILABILITY STATEMENT  Unclassified - Unlimited Subject Category: 07  Available electronically at <a href="http://gltrs.grc.nasa.gov">http://gltrs.grc.nasa.gov</a> This publication is available from the NASA Center for AeroSpace Information, 301-621-0390.			12b. DISTRIBUTION CODE	
13. ABSTRACT (Maximum 200 words)  The purpose of this study on micro-vane secondary flow control is to demonstrate the viability and economy of Response Surface Methodology (RSM) to optimally design micro-vane secondary flow control arrays, and to establish that the aeromechanical effects of engine face distortion can also be included in the design and optimization process. These statistical design concepts were used to investigate the design characteristics of "low unit strength" micro-effector arrays. "Low unit strength" micro-effectors are micro-vanes set at very low angles-of-incidence with very long chord lengths. They were designed to influence the near wall inlet flow over an extended streamwise distance, and their advantage lies in low total pressure loss and high effectiveness in managing engine face distortion. Therefore, this report examines optimal micro-vane secondary flow control array designs for compact inlets through a Response Surface Methodology.				
14. SUBJECT TERMS  Aeronautics; Propulsion; Fluid dynamics			15. NUMBER OF PAGES 44	
			16. PRICE CODE	
17. SECURITY CLASSIFICATION OF REPORT  Unclassified	18. SECURITY CLASSIFICATION OF THIS PAGE  Unclassified	19. SECURITY CLASSIFICATION OF ABSTRACT  Unclassified	20. LIMITATION OF ABSTRACT	